



HAL
open science

Structural Rearrangements of NR1/NR2A NMDA Receptors during Allosteric Inhibition

Marc Gielen, Anne Le Goff, David Stroebel, Jon W Johnson, Jacques Neyton, Pierre Paoletti

► **To cite this version:**

Marc Gielen, Anne Le Goff, David Stroebel, Jon W Johnson, Jacques Neyton, et al.. Structural Rearrangements of NR1/NR2A NMDA Receptors during Allosteric Inhibition. *Neuron*, 2008, 57 (1), pp.80-93. 10.1016/j.neuron.2007.11.021 . hal-01145410

HAL Id: hal-01145410

<https://hal.science/hal-01145410>

Submitted on 6 Mar 2018

HAL is a multi-disciplinary open access archive for the deposit and dissemination of scientific research documents, whether they are published or not. The documents may come from teaching and research institutions in France or abroad, or from public or private research centers.

L'archive ouverte pluridisciplinaire **HAL**, est destinée au dépôt et à la diffusion de documents scientifiques de niveau recherche, publiés ou non, émanant des établissements d'enseignement et de recherche français ou étrangers, des laboratoires publics ou privés.

Structural rearrangements of NR1/NR2A NMDA receptors during allosteric inhibition

Marc Gielen¹, Anne Le Goff¹, David Stroebel¹,
Jon W. Johnson², Jacques Neyton¹ and Pierre Paoletti¹

¹ Laboratoire de Neurobiologie
Ecole Normale Supérieure, CNRS
46 rue d'Ulm, 75005 Paris, France

² Department of Neuroscience
University of Pittsburgh
A210 Langely Hall
Pittsburgh, PA 15260, USA

Running title: Mechanism of NMDA receptor allosteric inhibition

Correspondence should be addressed to Dr. Pierre Paoletti, Laboratoire de Neurobiologie,
Ecole Normale Supérieure, 46 rue d'Ulm, 75005 Paris, France

Tel : 33 1 44 32 38 94 / Fax: 33 1 44 32 38 87 / email: paoletti@biologie.ens.fr

Key words: glutamate receptors, NMDA, zinc, desensitization, allosteric modulation

Acknowledgements: this work was supported by Ministère de la Recherche (MG), National Institute of Mental Health, NIH (JWJ), INSERM (PP) and ANR (PP).

SUMMARY

Ionotropic glutamate receptors (iGluR) subunits contain a large N-terminal domain (NTD) that precedes the agonist-binding domain (ABD) and participates in subunit oligomerization. In NMDA receptors (NMDARs), the NTDs of NR2A and NR2B subunits also form binding sites for the endogenous negative allosteric modulator Zn^{2+} ion. Although these allosteric sites have been characterized in detail, the molecular mechanisms by which the NTDs communicate with the rest of the receptor to promote receptor inhibition remain unknown. Here, we show that mutations that weaken hydrophobic or polar interactions at the heterodimer interface between NR1 and NR2A ABDs strongly increase zinc sensitivity of NR1/NR2A receptors, while mutations that strengthen dimer stability have opposite effects. A similar correlation is observed with proton inhibition, another form of allosteric modulation of NMDARs. Based on these results and on the recent analysis of AMPA receptor gating mechanisms, we propose that NR2A-NTD closure following zinc binding pulls the NR1/NR2A ABD dimer apart, which in turn enables proton binding and channel gate closure. Thus, conformational rearrangement at the ABD dimer interface appears to be a key mechanism conserved in all iGluR subfamilies. However, ABD dimer separation has evolved to fulfill different functions: fast desensitization at AMPA and kainate receptors, allosteric inhibition at NMDARs.

INTRODUCTION

In the vertebrate CNS, the amino-acid glutamate mediates fast excitatory neurotransmission by acting on iGluRs, which are integral membrane proteins containing glutamate-gated cation-permeable channels. iGluRs are subdivided into three subfamilies, AMPA, kainate and NMDA receptors (Dingledine et al., 1999). While AMPA and kainate receptors form a class of receptors endowed with fast kinetics and profound desensitization, NMDARs are distinguished by their slow kinetics and limited desensitization. Another distinctive feature of NMDARs is that their activity is tightly controlled by many endogenous substances. Among them, extracellular H^+ and Zn^{2+} ions, which act as allosteric inhibitors, are particularly interesting because they are likely to provide tonic inhibition of NMDARs under physiological conditions, suggesting an important role of these modulators in the control of neuronal excitability (Westbrook and Mayer, 1987; Traynelis and Cull-Candy, 1991; Paoletti et al., 1997; Vogt et al., 2000). In addition, during intense neuronal activity, increased NMDAR inhibition following rises in synaptic H^+ and Zn^{2+} concentrations (Traynelis and Chesler, 2001; Smart et al., 2004) may provide a way to limit NMDAR over-activation and therefore prevent neuronal injury. However, the structural basis by which these modulators exert their effects on NMDARs remains to be elucidated.

iGluRs have a characteristic modular architecture with each subunit containing four discrete domains (Mayer, 2006; Paoletti and Neyton, 2007): in the extracellular region, a tandem of large globular bilobate domains, the N-terminal domain (NTD) involved in subunit oligomerization followed by the agonist-binding domain (ABD) directly connected to the transmembrane part; a channel-forming domain comprising three transmembrane segments (TM1, 2 and 3) plus a re-entrant pore-loop (P); a cytoplasmic C-terminal domain involved in receptor trafficking at the synapse. Although iGluRs are tetrameric complexes, recent crystallographic and functional studies of the ABDs of AMPA and kainate receptors have revealed that these receptors operate as dimers of dimers. The bi-lobate ABDs of two adjacent subunits form dimers through back-to-back apposition of lobes 1, burying a large surface area involving extensive contacts between the two partner subunits (see Fig. 1). These studies have also established that the ABD dimer interface is a central structural element in the receptor gating process and have led to a comprehensive mechanistic model for receptor activation and desensitization. Agonist binding in the interlobe cleft of each ABD induces cleft closure, a movement that increases the separation between lobes 2 of the two adjacent subunits since their lobes 1 are “glued” together. According to the model, this separation, in turn, exerts some tension on the linkers connecting the ABDs to the transmembrane segments leading to opening of the ion channel. In the model, desensitization occurs when the dimer undergoes a conformational rearrangement that

involves the disruption of the lobe 1 dimer interface. This uncouples agonist-induced cleft closure from channel gate opening, allowing the ion channel to close while individual ABDs remain in their agonist-bound conformation (Sun et al., 2002; Jin et al., 2003; Horning and Mayer, 2004; Armstrong et al., 2006; Weston et al., 2006; Mayer, 2006). The recently solved structure of the NMDAR NR1/NR2A ABD heterodimer, which shows a strong structural conservation of the ABD dimer arrangement with that of non-NMDA receptors, indicates that the mechanism coupling ligand binding to channel gating is likely to be similar in NMDA receptors (Furukawa et al., 2005). However, in NMDARs, fast AMPAR-like desensitization does not occur and it is unknown if the ABD dimer interface rearranges during gating, and to what extent dimer stability influences channel activity.

In NMDARs, the NTDs are not only important for receptor assembly (Meddows et al., 2001) but also form binding sites for allosteric (non-competitive) ligands that modulate receptor activity. The NTDs of both NR2A and NR2B subunits bind the negative modulator Zn^{2+} with high (nM) and low (μ M) affinity, respectively (Choi and Lipton, 1999; Paoletti et al., 2000; Low et al., 2000; Rachline et al., 2005); in addition, the NR2B NTD binds the drug ifenprodil (Perin-Dureau et al., 2002). Results from site-directed mutagenesis experiments coupled to molecular modelling suggest that Zn^{2+} and ifenprodil bind the NTD interlobe central cleft and promote domain closure through a “clamshell-like” mechanism resembling the mechanism of action of glutamate at neighbouring ABDs. A major challenge is now to understand how the binding of a ligand at the very N-terminal regions of the receptor leads to ion channel closure. In the case of NR1/NR2A receptors, Low et al. (2000) have proposed that zinc inhibition proceeds through an enhancement of proton sensitivity. More recently, Mayer (2006) proposed a model in which NTD closure destabilizes the ABD dimer interface. This model, however, has not been experimentally tested, and therefore the mechanistic coupling between the NTDs and the gating machinery is still an open question. An intriguing side observation which attracted our attention is that NTD ligands, in parallel to their inhibitory effects on receptor activity, paradoxically *increase* receptor affinity for glutamate (Kew et al., 1996; Paoletti et al., 1997; Erreger et al., 2005). That is, NTD ligands promote entry into a state in which the receptor is inactive but has an increased affinity for the agonist, a feature that is a hallmark of desensitized states. Given the central importance of the dimer interface between adjacent ABDs in AMPA and kainate receptor desensitization, we investigated the role of the ABD interface in the allosteric modulation of NMDARs by NTD ligands. By introducing mutations at specific locations in the NR1/NR2A ABD dimer, we show that, in NR1/NR2A receptors, the ABD heterodimer interface has a pivotal role in the transduction pathway linking the NTDs to the channel gate and we propose a mechanistic scheme for allosteric regulation of NMDAR activity by the N-terminal modulatory domains.

RESULTS

Disruption of the hydrophobic contacts at the ABD dimer interface increases zinc sensitivity

The crystal structure of the isolated NR1/NR2A ABD heterodimer shows that both subunits are arranged in a “back-to-back” fashion that is similar to the arrangement of subunits in the non-desensitized state of the AMPA GluR2 ABD homodimer (Furukawa et al., 2005; Fig. 1). In particular, the NR1/NR2A ABD interface comprises numerous contacts made by residues found at -or in the vicinity of- helices α J and α D of both subunits, resulting in two subsites of dimerization: site A, formed by helix J of NR1 and helix D of NR2A; and site B, related to site A by a pseudo two-fold axis of symmetry, formed by the helix D of NR1 and helix J of NR2A. Both sites contain a cluster of highly conserved hydrophobic residues making numerous inter-subunit Van der Waals contacts that are expected to be important in dimer stabilization. We identified NR1-L777 and the homologous residue NR2A-L780 as residues likely to be essential for subunits dimerization since both leucines are buried at the core of the hydrophobic cluster with their side chain methyl groups involved in extensive hydrophobic contacts with the neighboring hydrophobic residues including NR2A-I514 and NR2A-S519 for NR1-L777, and NR1-A524 and NR1-I519 for NR2A-L780 (Fig. 2A). In addition, these two leucines are homologous to residue GluR2-L751 (Fig. 1B), mutation of which strongly promotes desensitization in GluR2 receptors (Horning and Mayer, 2004).

To explore the roles of NR1-L777 and NR2A-L780 in NMDAR zinc inhibition, we mutated each of these two leucine residues separately in alanine, whose shorter lateral chain should strongly disrupt the hydrophobic interface cluster. Compared to wild-type (wt) NR1/NR2A receptors, both NR1-L777A/NR2Awt and NR1wt/NR2A-L780A receptors display greatly enhanced zinc sensitivity (Fig. 2B-C). At 5 nM zinc, the lowest zinc concentration tested during initial mutation screening, currents were already strongly reduced (Fig. 2B). Whereas at wt NR1/NR2A receptors, zinc inhibits agonist-induced currents with an IC_{50} around 10 nM, in the mutated receptors, zinc IC_{50} was decreased by ~10-fold (1.1 and 1.2 nM for NR1-L777A/NR2Awt and NR1wt/NR2A-L780A receptors, respectively; Fig. 2C and Table 1). Another striking modification concerns the maximal level of zinc inhibition. Whereas, as previously reported, at wt NR1/NR2A receptors, saturating the high-affinity zinc binding site results in partial inhibition (maximal inhibition of 60-80%; Paoletti et al., 1997; Choi and Lipton, 1999; Low et al., 2000), at NR1-L777A/NR2Awt and NR1wt/NR2A-L780A receptors, residual currents in saturating zinc concentrations were dramatically diminished (maximal inhibition of 99% and 97%, respectively; Fig. 2C and Table 1). To make sure that

the observed inhibition was driven by zinc binding to the NR2A NTD and not to other potential sites of lower affinity located outside the NTD (see Rachline et al., 2005), we checked that high-affinity zinc inhibition was absent in receptors combining the NR1-L777A mutation with the NR2A-H128S mutation, a mutation that selectively abolishes zinc binding to the NR2A NTD (Fayyazuddin et al., 2000; Low et al., 2000; Paoletti et al., 2000). Indeed, 100 nM zinc, a concentration that induces an almost complete inhibition of NR1-L777A/NR2Awt receptors barely affected the doubly mutated NR1-L777A/NR2A-H128S receptors (relative current $93 \pm 3\%$ [n=3]).

To gain further insight into the importance of leucines NR1-L777 and NR2A-L780 in zinc inhibition of NMDARs, we introduced additional mutations at these positions. As expected from the introduction of polar residues in an hydrophobic cluster, substitutions by a serine or a cysteine induced a leftward shift in zinc sensitivity, similar to that observed with the alanine substitutions, with both an increase in zinc apparent affinity (IC_{50}) and “efficacy” (maximal level of inhibition) (Table 1). Interestingly, introducing a phenylalanine, a bulky hydrophobic residue, also strongly increased zinc sensitivity (Table 1). Of note, currents carried by NR1wt/NR2A-L780F were so small (< 40 nA, due to strong proton inhibition at pH 7.3; see below) that full zinc concentration-response curves could not be reliably obtained although it was clear that at these receptors zinc was very potent (>50% inhibition at 5 nM). Thus, the series of NR1-L777 and NR2A-L780 mutations reveal that perturbing the hydrophobic packing between the two adjacent ABDs, either by side chain truncation or change in hydrophobicity (A, C and S mutations), or through a likely steric clash (F mutation), markedly increases zinc sensitivity of NR1/NR2A receptors. These results also indicate that the two pseudo-symmetrical dimerization sites A and B contribute to a comparable extent to dimer stability, an observation that is not surprising given the strong sequence homology between the two protomers in regions constituting the dimer interface.

We next mutated the residues that, in the crystal structure, partner with leucines NR1-L777 and NR2A-L780 through intersubunit contacts. For each leucine, three interacting residues were identified: NR2A-I514, NR2A-E516 and NR2A-S519 for NR1-L777 and the homologous residues NR1-I519, NR1-N521 and NR1-A524 for NR2A-L780 (Fig. 2A). Each of these residues participates to the dimer interface stability by making an interdomain Van der Waals contact with the distal methyl group of the adjacent leucine. The influence of the interactions involving NR2A-E516 and NR1-N521 is difficult to evaluate by mutagenesis because these residues contact the corresponding leucine through their backbone $C\alpha$. A similar situation applies to NR2A-S519 with the involvement of its $C\beta$ methylene group that would only be eliminated with a substitution by glycine. Glycine substitutions, however, are known to disrupt secondary structures (O’Neil and DeGrado, 1990) and were therefore

avoided. Substituting isoleucine R1-I519 either by shorter aliphatic residues (valine or alanine) or by a large aromatic residue (phenylalanine) produced very modest effects on zinc sensitivity (Table 1). Similarly, receptors containing an alanine mutation at the homologous position in NR2A (NR2A-I514A) displayed unchanged zinc sensitivity compared to wt receptors (despite strong effects on agonist sensitivity; Table 1 and see Experimental Procedures). That valine can substitute for the isoleucine is not unexpected given that NR1-I519 contacts NR2A-L780 through its C β branch methyl group, an interaction which could be preserved in the valine mutant. In contrast, the results obtained with the alanine mutants are surprising since the one methyl side chain of the alanine is expected to be too short to form favourable Van der Waals contacts with the key leucines. Moreover, the homologous mutation GluR2-I481A has a strong effect on desensitization of AMPA receptors indicative of a much weakened dimer interface (Horning and Mayer, 2004). However, because GluR2 ABDs form homodimers with a two-fold symmetric dimerization, each individual mutation is present twice at the dimer interface while at heteromeric NMDARs, there is only one copy of the NR1 or NR2A mutation per heterodimer. Thus, to match more closely the AMPA receptor situation, we co-injected NR1-I519A with NR2A-I514A and found that doubly-mutated receptors displayed significantly enhanced maximal level of zinc inhibition compared to singly-mutated receptors in agreement with a significant decrease in stability of dimer contacts (Table 1). Introducing a charged aspartate at these positions also resulted in markedly enhanced zinc sensitivity, most particularly in the case of the NR1-I519D mutation, as expected for mutations that strongly disrupt the hydrophobic cluster (Table 1). Similarly, introducing charged residues at position NR1-A524 (D, E or K mutation) induced marked increase in zinc sensitivity (Table 1). Taken together, these results indicate that isoleucines NR2A-I514 and NR1-I519 as well as alanine NR1-A524 (and potentially NR2A-S519) are likely to contribute to dimer stability although some structural flexibility at the isoleucine positions can be supported without apparent destabilization of the interface.

The role of the hydrophobic interactions at the dimer interface in setting zinc sensitivity of NR1/NR2A receptors was further investigated by mutating additional residues of sites A and B in the vicinity of NR1-L777 and NR2A-L780. Residue NR1-L774 (site A) and the homologous residue NR2A-L777 (site B) on helices α J form the exterior side of the hydrophobic cluster and contact the methylene groups of residues from the adjacent subunit NR2A-E516 and NR2A-S519 (site A), and NR1-N521 and NR1-A524 (site B) (Fig. 2A). When NR1-L774 and NR2A-L777 were individually mutated to alanine, zinc sensitivity increased. In addition, when NR1-L774A was co-injected with NR2A-L777A, the corresponding doubly-mutated receptors displayed enhanced zinc sensitivity compared to the singly-mutated receptors (Table 1), reinforcing the importance of the ABD intermolecular Van der Waals

contacts in the control of zinc sensitivity. The shifts in sensitivity, however, were clearly not as marked as with NR1-L777 or NR2A-L780 mutated receptors. This is consistent with the fact that NR1-L774 and NR2A-L777 have their side chain partly solvent accessible and thus are expected to contribute significantly less than the other two leucines to dimer stability. Finally, we tested mutations at NR2A-V526. This residue, part of site B hydrophobic cluster, does not make direct contacts with the adjacent NR1 subunit but instead forms an intrasubunit contact with the key leucine 780 of NR2A (Fig. 2A). This latter interaction, however, is expected to be important for the ABD dimer assembly because of its likely involvement in the positioning of NR2A-L780. Consistent with this hypothesis, the alanine truncation mutant NR2A-V526A led to a small, but significant, increase in zinc sensitivity, while introduction of a less conservative mutation, NR2A-V526K strongly increased zinc sensitivity (Table 1).

Disruption of hydrogen bonds at the ABD dimer interface increases zinc sensitivity

Inspection of the NR1/NR2A ABD crystal structure indicates that, beside hydrophobic contacts, hydrogen bonds also participate to the stabilization of the ABD dimer interface. This is the case of residue NR1-E781 at the apex of helix J in site A. NR1-E781 is in a fully extended conformation and makes a bidentate contact with the base of helix D of the adjacent NR2A subunit very much like GluR2-E755 in AMPA receptors (Horning and Mayer, 2004). Residue NR1-E781 makes a direct hydrogen bond with the backbone amide nitrogen of NR2A-E516 and a hydrogen bond with the backbone amide nitrogen of NR2A-E517 via a water molecule (Fig. 3A). The favourable electrostatic interaction between the negatively charged glutamate and the dipole of the α D helix of NR2A, may also contribute to the dimer interface cohesion. To remove these interactions, NR1-E781 was first substituted into alanine. This resulted in a marked enhancement of zinc sensitivity with an effect on both zinc IC_{50} and the maximal level of zinc inhibition (Zn IC_{50} of 2.4 nM and maximal inhibition of 92% [n=9], Table 1). When the glutamate side chain was replaced by a more conservative aspartate, a shorter negatively charged residue that should weaken both hydrogen bond network and charge-dipole interaction, zinc sensitivity was increased but to a lesser extent (Table 1). Surprisingly, replacing NR1-E781 by a glutamine, a neutral residue of similar length which should permit formation of one hydrogen bond with the neighbouring D helix but not the charge-dipole interaction, strongly increased zinc sensitivity (Zn IC_{50} of 1.3 nM and maximal inhibition of 97% [n=8], Fig. 3B). This result suggests that the charge-dipole interaction between NR1-E781 and the NR2A α D helix may contribute to the overall dimer stability. The fact, however, that the Q mutation has a “stronger” phenotype than the A mutation is difficult to explain assuming that the sole effect of the mutation is to weaken

dimer stability and likely reflects additional effects of the Q mutation on other conformational state(s) of the dimer (possibly through stabilization of a “desensitized” state; see Armstrong et al., 2006). In conclusion, the hydrogen bond network at the ABD dimer interface appears to be an important structural determinant involved in the control of the zinc sensitivity of NR1/NR2A receptors most likely by contributing to the stability of the ABD dimer interface.

Receptors with cysteine cross-linked ABDs display redox-state dependent zinc sensitivity

A prediction based on the preceding results showing that disrupting the intersubunit ABD dimer contacts enhances zinc sensitivity is that strengthening dimer stability should also affect zinc sensitivity. We first tried to increase dimer stability by introducing either a) polar residues to mimic the intersubunit salt links present in AMPA and kainate ABDs (Horning and Mayer, 2004; Priel et al., 2006; Plested and Mayer, 2007), b) tyrosines to mimic the non-desensitizing GluR2-L483Y receptor situation (Sun et al., 2002; Furukawa et al., 2005), or c) mutations to consolidate the hydrogen bond network between the two partner subunits. Disappointingly, introducing polar residues or tyrosines produced either no significant change in zinc sensitivity (NR1-S773N/NR2A-S519E, NR1-N521Y/NR2A-E516Y) or increased zinc sensitivity (NR1-A524E/NR2A-V526K-D776N) (Table 1). In contrast, introducing H-bond acceptor groups at position NR2A-G784 (homologous to NR1-E781) did result in a small, but significant, decrease in zinc sensitivity (Table 1 and Fig. S1) suggesting that enhanced dimer stability may render zinc inhibition less potent.

To test the influence of dimer stabilization on zinc sensitivity more directly, we used an approach based on engineered disulfide bridges. In their study of the NR1/NR2A ABD structure, Furukawa et al. (2005) showed that it is possible, in full-length receptors, to cross-link adjacent NR1 and NR2A subunits by introducing two pairs of cysteines at appropriate positions in the ABD NR1/NR2A heterodimer interface (NR1-N521C-L777C and NR2A-E516C-L780C, hereafter named NR1-CC and NR2A-CC, respectively; see Fig. 4A). By performing Western blot experiments on whole oocyte extracts, we first verified that in our hands and only under non-reducing conditions, such doubly-cysteine mutated NR1 and NR2A subunits do form heterodimers in an intact receptor (Fig. S2). We then assessed zinc sensitivity of NR1CC/NR2A-CC receptors under different redox conditions. In control conditions (i.e. before any redox treatments), NR1-CC/NR2A-CC receptors exhibited a maximal zinc inhibition significantly lower than that observed on NR1wt/NR2Awt receptors (64% vs 81%; Fig. 4B-C) as would be expected if a significant proportion of surface NMDA receptors has a reduced zinc sensitivity because of restrained conformational mobility of

covalently-attached ABDs. We obtained further evidence that this is likely to be the case by treating the oocytes with DTNB, an oxidizing agent that promotes disulfide bond formation. As shown in Figure 4B-C, DTNB treatment strongly reduced the sensitivity to zinc, as judged by the much lowered maximal level of inhibition (37%). The fact that zinc sensitivity of DTNB-treated receptors was not completely abolished may be due either to a limited access of DTNB to the dimer interface resulting in a mixed population of receptors with reduced and intact cross-links or to insufficient time of treatment. Another possibility could be that even in the cross-linked receptors, some movements at the ABD interface are still possible following zinc binding to the NTD. Whatever the explanation, we predicted that breaking the engineered disulfide bonds should restore zinc sensitivity. Consistent with this idea, DTE treatment (5 mM, 15 min) dramatically increased zinc sensitivity (100% maximal inhibition; Fig. 4B-C). The sensitivity of DTE-treated R1-CC/2A-CC receptors to zinc was in fact similar to that of receptors harbouring a single cysteine mutation at the corresponding α J helix leucine positions (R1-L777C/2Awt or R1wt/2A-L780C receptors; see Table 1) as expected if most of the disulfide bonds have been cleaved by the DTE treatment. To verify that the observed effects resulted from a selective modification of the two disulfide bonds introduced at the subunit interface, we performed similar redox treatments on oocytes expressing either wt NR1/NR2A receptors or receptors containing only one set of double cysteine mutations, which do not give rise to disulphide-linked NR1/NR2A heterodimers (R1-CC/2Awt and R1wt/2A-CC receptors; Fig. S2). As shown in Fig. 4D, none of the redox treatments affected the maximal level of zinc inhibition of these receptors. Finally, we also found that it was possible to reversibly switch NR1-CC/NR2A-CC receptors from a low- to a high-zinc sensitivity state by sequential applications of DTNB and DTE (Figs 4B and D). These results reveal that cross-linking ABD protomers leads to receptors with greatly diminished zinc sensitivity and support a model in which conformational rearrangements of the agonist binding cores are required to couple zinc binding to the NTD to subsequent channel closure.

Disruption of the heterodimer interface between ABDs increases proton sensitivity

A distinctive property of the high-affinity zinc inhibition of NR1/NR2A receptors is that it saturates at a maximal level of 60-80% (Paoletti et al., 1997; Choi and Lipton, 1999; Low et al., 2000). Based on the observation that the extent of maximal zinc inhibition depends on extracellular pH (inhibition by a saturating zinc concentration increases as proton concentration increases), it has been proposed that zinc exerts its inhibitory action on NR1/NR2A receptors through an enhancement of tonic proton inhibition (Choi and Lipton, 1999; Low et al., 2000). According to this model, the presence of protons is required for zinc inhibition to occur. The residual current observed at saturating zinc concentrations and at

physiological pH reflects the fact that saturating the high-affinity zinc binding site does not lead to saturation of the inhibitory proton binding site at pH 7.3. Given the strong effects of the ABD dimer interface mutations on zinc sensitivity, and in particular on the maximal level of zinc inhibition, we decided to examine the pH sensitivity of our mutant receptors. We found that mutation of the central leucines of the ABD interface hydrophobic cores, which greatly enhanced maximal zinc inhibition (see Fig. 2), dramatically increased proton sensitivity. Thus, as illustrated in Figure 5A, switching the agonist solution from pH 7.3 to 8.3, which results in a modest 1.15-fold increase of wt currents, induced a 4- and 2.6-fold increase of currents carried by NR1-L777A/NR2Awt and NR1wt/NR2A-L780A receptors, respectively. Currents from mutant receptors were still profoundly inhibited by H⁺ at pH 8.3 since further potentiation could be induced by increasing pH to 9.3 (Fig. 5A). Using the series of mutations that we had produced at these positions, we found that the potentiation was largest for NR1/NR2A-L780F receptors with a remarkable 30-fold increase in current amplitude when jumping from pH 7.3 to 9.3 (Fig. 5A). Performing full concentration-response curves revealed that pH sensitivity of these mutant receptors was shifted by more than two orders of magnitude in comparison to wt receptors (pH of IC₅₀ of 9.13 [n=4-7] for NR1-L777A/NR2Awt receptors, 9.16 [n=4-8] for NR1wt/NR2A-L780A receptors and 9.08 [n=4] for NR1/NR2A-L780F receptors, vs 6.92 [n=14] for wt receptor; Fig. 5B).

To obtain a more complete view of the relationship between zinc and proton sensitivities at NR1/NR2A receptors, we measured pH sensitivity of many dimer interface mutants covering a large spectrum of zinc sensitivity (Table 1). Mutant receptors that displayed enhanced zinc sensitivity also displayed enhanced pH sensitivity. Two mutant receptors deviated from this general trend: NR1-I519D/NR2Awt which showed unusual biphasic pH sensitivity (with a potentiating and an inhibitory component; data not shown) and NR1-A524E/NR2Awt (and to a lesser extent NR1-A524D/NR2Awt) which showed very little shift in pH sensitivity despite a marked increase in zinc sensitivity. We believe that for these mutants, the “abnormal” pH sensitivity reflects the presence of an additional pH effect involving highly perturbed pKa's of the introduced carboxylic groups (probably because of the clustering of multiple charged residues in a relatively low polar environment; see Fersht, 1999). Notwithstanding these latter mutants, we found that the maximal level of zinc inhibition and proton sensitivity were strongly correlated (Fig. 6). This result agrees well with a model in which NTD-controlled zinc inhibition results from an enhancement of proton inhibition and indicates that common mechanisms are likely to operate during zinc and proton inhibition.

We gained additional evidence for a functional interaction between the ABD dimer interface and the NTDs by measuring pH sensitivity of receptors combining a NR1 ABD

interface mutation (NR1-E781A) with a NTD-deleted NR2A subunit (NR2A-deINTD; see Rachline et al., 2005). Although the interface mutation or the NTD deletion separately caused a modest enhancement of proton sensitivity (pH of IC₅₀ of 7.3 and 7.2, respectively; Table 1 and Fig. S3), the combination of both modifications resulted in a strong synergistic increase in proton sensitivity (pH of IC₅₀ of 9.1; Fig. S3).

Increased accessibility of the ABD dimer interface upon zinc inhibition

Mutations expected to weaken (or strengthen) ABD dimer stability selectively enhance (or decrease) zinc and proton sensitivities of NR1/NR2A receptors. This observation strongly suggests that disruption of the ABD dimer interface, with one protomer moving away from the other, constitutes a central conformational rearrangement occurring during zinc and proton inhibitions, very much like the movement occurring during AMPA and kainate receptor desensitization (Armstrong et al., 2006; Weston et al., 2006; Priel et al., 2006). To probe for this putative conformational change, we introduced a cysteine residue at the ABD dimer interface and compared the rate of modification of the mutant receptors by the thiol modifying agent sodium (2-sulfonatoethyl)methane thiosulfonate (MTSES) with and without zinc. We hypothesized that attachment of the bulky (2-sulfonatoethyl)methane moiety at the ABD interface of the mutated receptors would increase their sensitivity to zinc and pH, thereby decreasing current sizes. According to a model in which the ABD interface becomes more accessible upon zinc inhibition, the rate of MTSES modification should be faster in zinc than without. We chose to introduce the cysteine substitution at position 2A-V526 because of the following criteria: first, this residue, as judged by the NR1/NR2A ABD dimer crystal structure (Furukawa et al., 2005), is poorly accessible to the bulk solvent in the “resting” state of the ABD dimer; second, its mutation to cysteine has only a very minor effect on zinc sensitivity (Zn IC₅₀ = 10.9 nM and maximal inhibition of 81%, [n = 3]) such that residual currents in saturating zinc concentrations are of large enough amplitude to be accurately measured; third, its replacement by a large charged residue such as a lysine induced a marked increase in zinc sensitivity (see Table 1) presumably through disruption of the dimer interface; fourth, in GluR2 AMPA receptors, the homologous residue (K493) becomes more exposed to the solvent during receptor desensitization (Armstrong et al., 2006).

We observed that the reduction of currents carried by NR1wt/NR2A-V526C receptors induced by MTSES application was both faster and of greater amplitude in the presence of zinc (applied at 500 nM, a saturating concentration) than in its absence (Fig. 7A-B). The enhanced magnitude of inhibition (61 ± 4% [n = 4] inhibition in zinc vs 39 ± 4% [n = 5] in DTPA) is expected if in both situations, the decrease in currents induced by MTSES reflects

a similar enhancement of proton inhibition but starting from receptors under higher tonic proton inhibition in the zinc conditions (see Low et al., 2000). From a kinetic point of view, in both cases, application of MTSES was best described by a two-component time course. Since the fast component, but not the slow one, was also observed during treatment of NR1wt/NR2Awt receptors with MTSES (most likely due to modification of an endogenous cysteine; data not shown), we concentrated our analysis on the slow component. On average, this latter component was 1.9-fold faster in the presence of zinc than in its absence (Fig. 7C-D). Thus, the thiol moiety of the interface residue 2A-V526C becomes more accessible upon NTD-driven zinc inhibition.

Discussion

Using the X-ray crystal structure of the NR1/NR2A agonist-binding domain dimer (Furukawa et al., 2005), we created a series of mutants specifically designed to affect the stability of the ABD dimer interface. Characterization of these mutants revealed that the ABD dimer interface is a key structural determinant that permits functional coupling between the NTDs and the pore region. Our data also reveal that the ABD dimer interface controls proton sensitivity. Our results establish that intersubunit contacts between the ligand binding cores of NR1 and NR2A subunits undergo significant conformational rearrangements during zinc and proton inhibitions. There are striking similarities between the effects of our mutants on zinc (and proton) modulation and the previously described effects of homologous ABD dimer interface mutants on AMPA and kainate receptor desensitization. Whereas in AMPA and kainate receptors, destabilization of the interface increases the speed and extent of desensitization (Sun et al., 2002; Horning and Mayer, 2004; Weston et al., 2006; Priel et al., 2006; Armstrong et al., 2006; Plested and Mayer, 2007), we show here that in NMDA NR1/NR2A receptors, weakening the intersubunit ABD contacts selectively enhances sensitivity to allosteric inhibitors. Accordingly, we propose a model for the negative allosteric modulation of NR1/NR2A receptors centered on the idea that zinc- or proton-inhibited NR1/NR2A receptors “resemble” AMPA (or kainate) desensitized receptors (Fig. 8; see also Mayer, 2006). In this model, zinc inhibition proceeds through a sequence of molecular events involving three distinct “modules” of the receptor: the N-terminal domain (the locus of zinc binding); the agonist-binding domain; and ultimately the transmembrane region. First, zinc binds the central cleft of NR2A NTDs (shown following agonist binding in Fig. 8 as state 1) and promotes domain closure by stabilizing a closed-cleft conformation (Paoletti et al., 2000; Fig. 8, state 2). Second, closure of the NTDs exerts tension on the linker connecting the NTDs to the ABDs, destabilizing the ABD dimer assembly and enhancing proton site affinity. Third, pulling apart of the ABD protomers together with proton binding relieve strain on the linkers connected to the transmembrane segments, allowing the channel to close, even though the agonists remain bound to the receptors.

Our model explains why mutations that weaken ABD dimer stability increase zinc inhibition, whereas cross-linking the two ABD protomers through disulfide bridges has an opposite effect. This model accounts for the strong correlation between pH and zinc modulations (Low et al., 2000 and Fig. 6) since, in the inhibition transduction cascade, proton binding takes place downstream of zinc-induced closure of the NTDs. This model also accounts for the increased glutamate affinity induced by zinc inhibition at the NTD (Paoletti et al., 1997; Erreger et al., 2005), since separation of the agonist-bound ABDs relieves the strain exerted by the linkers from the transmembrane segments, thus stabilizing the closed

conformation of the ABDs. Finally, this model highlights the key importance of dimer interfaces in glutamate receptor-channel activation and modulation. During iGluR activation, agonist-induced closure of the ABDs pulls open the channel gate because the ABDs are attached together through their lobes 1 while lobes 2 are able to move (Mayer, 2006). We suggest that during NMDA receptor modulation, the zinc-induced closure of the NTDs can be transduced into ABD dimer separation because the NTDs are similarly attached one to the other through their first lobes (Fig. 8; see Madry et al., 2007). Supporting this hypothesis, AMPA receptor NTDs are known to dimerize (Kuusinen, 1999; Ayalon et al., 2005), and crystal structures from structurally-related domains found in metabotropic glutamate receptors consistently show that the dimer interface is generated exclusively by lobe 1 contacts (Jingami et al., 2003).

Although our model provides a description of the cascade of structural reorganizations coupling the NTDs to the gating machinery, several questions remain open that suggest future experimental directions. For example, it is yet unclear if in NR1/NR2A receptors, the NTDs assemble as heterodimers as do the ABDs, or alternatively as homodimers. We favor the heterodimeric arrangement because it maintains the overall quaternary arrangement seen at the level of the ABDs (Furukawa et al., 2005). One then must assume that, in a NR1/NR2A heterodimer unit, occupancy of a single NR2A NTD high-affinity zinc-binding site is sufficient to trigger the conformational changes required for inhibition. The NR1-NTD, presumably unliganded, could close with NR2A in a concerted transition, remain in an open conformation, or be constitutively closed. The fact that triheteromeric NMDA receptors containing a single NR2A subunit (NR1/NR2A/NR2B or NR1/NR2A/NR2C receptors) retain a high-sensitivity to zinc (but show a decreased maximal level of inhibition; Hatton and Paoletti, 2005) demonstrates that the binding energy resulting from occupancy of a single NTD zinc-binding site in the tetramer is sufficient to shift the equilibrium towards an increased proportion of inactive receptors.

Another question that remains to be solved is why a saturating zinc concentration does not fully inhibit NR1/NR2A NMDA receptors. According to Low et al. (2000), it is because zinc does not lead to the saturation of the proton binding site. But then, why does it not? It could be that only a fraction of receptors with bound zinc have the NTD closed. In other words, zinc binding may not obligatorily lead to NTD closure, but just shifts the equilibrium between NTD-open and NTD-closed conformations toward the NTD-closed conformation (equilibrium between states 1 and 3, Fig. 8). Another possibility is that closure of the NTD affects the ABD dimer conformation of only a fraction of receptors. Uncoupling between NTD closure and ABD dimer separation could be due to structural rearrangements of the linker region between the NTD and the ABD. The incompleteness of zinc inhibition

would then reflect a competition between two interfaces, the NTD/ABD *intra*-subunit interface and the ABD/ABD *inter*-subunit interface (assuming that disruption of the latter is required for receptor inhibition) (equilibrium between states 2 and 3, Fig. 8). Whatever the mechanism, it is interesting to note that the incompleteness of zinc inhibition contrasts with the almost complete extent of desensitization at AMPARs upon dimer interface disruption (Sun et al., 2002). The mechanical constraints that the NTDs exert on the ABDs may significantly differ between the two receptor types. Our observation that the NR2A-NTD deletion acts synergistically with an ABD dimer interface mutation on proton sensitivity argues that in NMDARs, the NR2A-NTD, at least in its open conformation, may help stabilizing the ABD dimer.

Our findings that mutations that increase zinc sensitivity also increase proton sensitivity agree with the proposal of Low et al. (2000) that high-affinity zinc inhibition of NR1/NR2A receptors proceeds through an enhancement of tonic proton inhibition. The observed ~2-fold increase in the speed of MTSES modification (Fig. 7) is consistent with the observation that saturation of the high-affinity zinc site causes a 0.7 pH unit alkaline shift of the proton inhibition curve of NR1/NR2A receptors (Low et al., 2000). At pH 7.3, a 0.7 unit increase in pH sensitivity would approximately double the fraction of receptors inhibited by protons (from 30 to 60% of the total receptor population), which in our model are the receptors that are amenable to MTSES modification. Moreover, our observation that NR1/NR2A receptor mutations that disrupt the ABD dimer interface strongly enhance proton sensitivity provides the important mechanistic insight that proton inhibition involves separation of the ABDs. Remarkably, in AMPARs, external acidification has been shown to enhance desensitization, whereas adding cyclothiazide, a compound that stabilizes the ABD dimer assembly (Sun et al., 2002), strongly reduces pH sensitivity (Ihle and Patneau, 2000; Lei et al., 2001). Thus we propose that breaking the ABD dimer interface is a general mechanism underlying proton modulation of the iGluRs. Whether ABD separation is required for proton to access its binding site or proton binding occurs prior ABD separation remains an open question. The exact location of the proton binding site also remains to be determined. Based on mutagenesis experiments similar to ours, Low et al. (2003) have suggested that this site is closely associated to the transmembrane segments. However, our results suggest that protons could as well bind at the ABD dimer interface.

In conclusion, by determining how distal N-terminal domains communicate in intact NR1/NR2A receptors with the agonist-binding and gating machinery, our work reveals the molecular mechanisms by which two naturally-occurring modulators of NMDARs, the H⁺ and Zn²⁺ ions, control receptor activity. Together with previous studies on AMPA and kainate receptors, our results establish that the ligand-binding core dimer is central in regulating

channel activity in the entire iGluR family. Conformational changes at subunit-subunit interfaces are thus critical events for iGluR function, an idea that is now emerging as a general theme in the large family of multimeric neurotransmitter receptors (Sine & Engel, 2006).

Experimental Procedures

Molecular Biology

The pcDNA3-based expression plasmids for NR1-1a (named NR1 herein) and NR2A (all rat clones), the mutagenesis strategy and sequencing have been described previously (Rachline et al., 2005).

Electrophysiology

Recombinant NMDA receptors were expressed in *Xenopus laevis* oocytes after co-injection of cDNAs (at 10 ng/ μ l; nuclear injection) coding for the various rat NR1 and NR2A subunits (ratio 1:1). Oocytes were prepared, injected, voltage-clamped and superfused as described previously (Paoletti et al., 1995, 1997). For all experiments, except for those aimed at measuring the pH sensitivity (see below), the standard external solution contained (in mM): 100 NaCl, 0.3 BaCl₂, 5 HEPES. The pH was adjusted to 7.3 with KOH.

For free zinc concentrations in the 1 nM-1 μ M range, tricine (10 mM) was used to buffer zinc (Paoletti et al., 1997) and the following relationship was used to calculate the free zinc concentrations: $[Zn]_{free} = [Zn]_{added} / 200$ (Fayyazuddin et al., 2000). In the control "0" added zinc solution, the heavy metal chelator DTPA (10 μ M) was present in addition to tricine. For the zinc concentration-response curves of the mutant receptors displaying a very high zinc sensitivity (Figs 2 and 3), zinc was not buffered with tricine but with ADA (1mM) and the following equation was used to calculate free zinc concentrations ($[Zn]_{free} = [Zn]_{added} / 17000$; Fayyazuddin et al., 2000). For the pH sensitivity experiments, an enriched HEPES external solution was used to insure proper pH buffering. This solution contained (in mM): 60 NaCl, 2.5 KCl, 40 HEPES. pH was first adjusted to 10.3 with NaOH. More acidic solutions were then obtained by decreasing pH with concentrated HCl. This procedure was chosen because it maintains Na⁺ concentration at a constant value irrespective of the pH. To chelate trace amounts of contaminant zinc, DTPA (10 μ M) was added in all the solutions used for pH experiments.

NMDA currents were induced by simultaneous application of saturating concentrations of L-glutamate and glycine (agonists). These concentrations were set at 100 μ M each for wt receptors. However, since, at NR1/NR2A receptors, both Zn IC₅₀ and maximal inhibition depend on the concentration of glutamate used to activate the receptors (with stronger inhibition with increased glutamate concentrations; Zheng et al., 2001; Erreger et al., 2005), special care was taken to estimate, for each mutant receptor, the appropriate

glutamate concentration required to maximally activate the receptors. For NR1-L777A/NR2Awt and NR1wt/NR2A-L780A receptors, which display the strongest shifts in zinc sensitivity, full agonist dose-response curves were performed, revealing agonist sensitivity close to that of wt receptors (Fig. S4). Accordingly, 100 μ M glutamate (together with 100 μ M glycine) was used with these receptors. For all other mutants, currents elicited by 100 μ M and 1 mM agonists were initially compared. If these currents differed by less than 15% (as observed with wt receptors), glutamate and glycine were used at 100 μ M each. This was the case for most of the mutants described in the present study. For mutant receptors displaying a larger difference (NR1wt/NR2A-I514A, NR1wt/NR2A-I514D, NR1-CC/NR2A-CC), full agonist concentration-response curves were performed (Figs S5 and S6) and, in the following zinc/pH experiments, glutamate and glycine concentrations were adjusted to provide maximal or nearly maximal activation of the receptors (1 mM glutamate and glycine for NR1-CC/NR2A-CC, 100 μ M glycine + 1 mM glutamate for NR1wt/NR2A-I514A, 100 μ M glycine + 10 mM glutamate for NR1wt/NR2A-I514D).

When performing full pH concentration-response curves, at very alkaline pH values, agonist concentrations were adjusted to compensate for the loss of protonation of the α -amine moiety (pKa \sim 9.7 for both L-glutamate and glycine). Thus, at pH 9.3, 9.8 and 10.3, glutamate and glycine concentrations were increased by 1.4 fold, 2.1 fold and 5 fold, respectively. At all other pH values, agonist concentrations were kept identical to those used at pH 7.3.

Currents were measured at a holding potential of -60 mV and experiments were done at room temperature. Error bars represent the standard deviations of the mean relative currents.

Redox treatments of receptors with engineered disulphide bonds

Since NR1-CC/NR2A-CC receptors exhibit lower agonist affinities compared to wt receptors (Furukawa et al., 2005 and Fig. S6), agonist concentrations had to be increased from 100 μ M (wt receptors) to 1 mM when studying these receptors in order to be at saturating concentrations. This was also the case for NR1wt/NR2A-CC receptors. To promote disulfide bridge cleavage, oocytes were incubated with the reducing agent DTE (5 mM) in a Barth solution containing (in mM): 88 NaCl, 1 KCl, 0.33 Ca(NO₃)₂, 0.41 CaCl₂, 0.82 MgSO₄, 2.4 NaHCO₃, 10 HEPES supplemented with gentamycin (50 μ g/mL) and the NMDAR antagonist D-APV (50 μ M) to prevent NMDAR-induced cell toxicity. pH was adjusted to 8.0. To induce the formation of disulfide bonds, oocytes were incubated with the oxidizing agent DTNB (0.5

mM) in the same Barth solution supplemented with gentamycin, D-APV and the heavy-metal chelator DTPA (10 μ M).

Immunoblotting

Xenopus oocytes were prepared and injected as for the electrophysiological experiments. After 2-5 days, expression level for NMDA receptors was checked using two-electrode voltage clamp and only oocytes that showed NMDA currents >300 nA were subsequently used. Oocytes were first treated with 0.5 mM DTNB for 5 min. They were then homogenized in a buffer (10 μ l/cell) containing 20 mM Tris-HCl (pH 8.0), 50 mM NaCl, 1/100 volume of mammalian protease inhibitor cocktail (Sigma) and 1 mM *N*-ethylmaleimide. After centrifugation (12,200 g for 10 min at 4°C), the pellet was then solubilized in the same buffer complemented with 1% β -D-dodecyl-maltoside (Anatrace). Sample amounts equivalent to two oocytes were loaded on 8% gels (SDS-PAGE) either in presence or absence of 100 mM DTE. Gels were incubated 10 min in 1 mM DTE before transfer on PVDF membranes. PVDF membranes were blocked with fat-free milk (5% in TBS-Tween buffer) and incubated overnight (4°C) with 1/2,000 dilution of mouse anti-NR1 antibody (amino acids 660-811, Chemicon) followed by 1/5,000 HRP-conjugated goat anti-mouse secondary antibody and revealed with SuperSignal West Pico Kit (Pierce).

Data Analysis

Data were collected and analyzed using Clampex 7.0 and Clampfit 9.2 (Axon Instruments, Foster City, CA). Data were fitted using KaleidaGraph 4.0 (Synergy Software, Reading, PA). For zinc concentration-response curves, the experimental data points were fitted with the following Hill equation: $I_{Zn}/I_{Control} = 1 - Inhib_{max} / (1 + (IC_{50}/[Zn])^{nH})$, where $I_{Zn}/I_{Control}$ is the mean relative current, [Zn] is the concentration of free zinc, nH is the Hill coefficient, $Inhib_{max}$ is the maximal zinc inhibition, and IC_{50} is the concentration of zinc producing 50% of the maximal inhibition. IC_{50} , $Inhib_{max}$, and nH were fitted as free parameters.

When performing pH experiments, we observed that changes in pH of the extracellular solution leads to small (a few mV) but significant changes in the potential of the bath reference electrode, an effect which results in small shifts of the reversal potential of NMDA responses. To correct for these effects, the measured NMDA current values were multiplied by the following factor: 0.97 at pH 6.3, 0.98 at pH 6.8, 1.03 at pH 7.8, 1.05 at pH 8.3, 1.07 at pH 8.8, 1.08 at pH 9.3, 1.09 at pH 9.8 and 10.3. To generate pH concentration-response curves, a two step procedure was used. For each cell, the experimental data points

were first fitted using the following Hill equation: $I_{pH}/I_{Control} = b / (1+10^{(n_H (pH_{IC50}-pH))})$, where $I_{pH}/I_{Control}$ is the relative current (control current is obtained at pH 7.3), b is the maximum potentiation obtained at alkaline pH, pH_{IC50} is the pH producing 50% of inhibition, and n_H is the Hill coefficient. pH_{IC50} , n_H , and b were fitted as free parameters. For each cell, all data points were then divided by b to have a maximum relative current normalized to 1. Resulting values obtained for each individual cell and for each pH were then averaged and the mean data points were then fitted with the same Hill equation as above but with b fixed to 1.0.

To calculate the ΔG of maximal zinc inhibition (ΔG°_{Zn}), we assumed that, at the plateau of the zinc-concentration response curve (i.e. at saturating zinc concentrations), the agonist-bound receptors are in equilibrium between two states, a zinc-bound inactive state (RZn) and a zinc-bound active state (RZn*). Thus, the equilibrium constant K_{Zn} between these two states is given by $K_{Zn} = [RZn^*] / [RZn] = (1 - Inhib_{max}) / Inhib_{max}$ (with $Inhib_{max}$ being the maximal inhibition produced by zinc; see above) and the corresponding Gibbs free energy (ΔG°_{Zn}) is defined as: $\Delta G^{\circ}_{Zn} = -RT \ln(K_{Zn}) = -RT \ln(10) \log((1 - Inhib_{max}) / Inhib_{max})$, with R being the gas constant and T the absolute temperature. As an approximation, we used ΔG°_{Zn} (kcal.mol⁻¹) = - 1.4 $\log((1 - Inhib_{max}) / Inhib_{max})$ at room temperature. For each mutant receptor (mut), we then calculated the difference $\Delta \Delta G^{\circ}_{Zn}(mut) = \Delta G^{\circ}_{Zn}(mut) - \Delta G^{\circ}_{Zn}(wt)$, where $\Delta G^{\circ}_{Zn}(wt)$ is the ΔG of maximal zinc inhibition for wt receptors expressed in the same batch of oocytes as the studied mutant. We used this procedure to circumvent some variability seen in the maximal level of zinc inhibition at wt NR1/NR2A receptors (max. inhibition 0.77-0.83 range). To quantify proton inhibition, we used the equilibrium constant K_H between the protonated (inactive) and deprotonated (active) state of the agonist-bound receptor to calculate the corresponding free energy: $\Delta G^{\circ}_{pH} = -RT \ln(K_H) = RT \ln(10) pH_{IC50}$. At room temperature and at pH 7.3, we used ΔG°_{pH} (kcal.mol⁻¹) = 1.4 pH_{IC50} . For consistency with the analysis of the maximal zinc inhibition, the difference $\Delta \Delta G^{\circ}_{pH}(mut) = \Delta G^{\circ}_{pH}(mut) - \Delta G^{\circ}_{pH}(wt)$ was then calculated for each mutant receptor. Of note, K_H accounts for a binding equilibrium, whereas K_{Zn} accounts for an equilibrium between two zinc-bound states and thus does not involve any binding step.

Chemicals

HEPES, L-glutamate, glycine, DTPA (diethylenetriamine-pentaacetic acid), Tricine (N-tris(hydroxymethyl)methylglycine), ADA (N-[2-Acetamido]-2-iminodiacetic acid), DTE (dithioerythritol) and DTNB (5,5'-dithio-bis(2-nitrobenzoic acid)) and NEM (N-ethylmaleimide) were obtained from Sigma (Saint-Louis, MO, USA), D-APV (D-(-)-2-Amino-5-phosphonopentanoic acid) from Ascent Scientific (Weston-Super-Mare, UK), gentamycin

from Gibco (Invitrogen, Rockville, MD, USA) and sodium (2-sulfonatoethyl)methane thiosulfonate (MTSES) from Toronto Research Chemicals (North York, On., Canada). L-glutamate and glycine stock solutions (100 μ M - 1 M) were prepared in bi-distilled water. DTNB was prepared as a stock solution (50 mM) in an HEPES solution (500 mM, pH 8.0) whereas DTE was freshly prepared directly from powder. MTSES was prepared as 200 mM stock solutions in bi-distilled water, aliquoted in small volumes (200 μ L) and immediately frozen at -20°C; aliquots were thawed just before use and replaced every 30 min. Zinc was added as chloride salts (ZnCl_2 , ACS reagent quality, Sigma) by dilution from 100 mM stock solutions prepared in 10^{-2} N HCl.

3D structure illustrations

Figures from the crystal structure of the NR1/NR2A ABD heterodimer (pdb coordinates 2A5T; Furukawa et al., 2005) were prepared with PyMOL (DeLano, 2002).

REFERENCES

- Armstrong, N., Jasti, J., Beich-Frandsen, M., and Gouaux, E. (2006). Measurement of conformational changes accompanying desensitization in an ionotropic glutamate receptor. *Cell* **127**, 85-97.
- Ayalon, G., Segev, E., Elgavish, S., and Stern-Bach, Y. (2005). Two regions in the N-terminal domain of ionotropic glutamate receptor 3 form the subunit oligomerization interfaces that control subtype-specific receptor assembly. *J Biol Chem* **280**, 15053-15060.
- Choi, Y. B., and Lipton, S. A. (1999). Identification and mechanism of action of two histidines residues underlying high-affinity Zn²⁺ inhibition of the NMDA receptor. *Neuron* **23**, 171-180.
- DeLano, W. L. (2002) The PyMOL Molecular Graphics System. DeLano Scientific, San Carlos, CA, USA.
- Dingledine, R. J., Borges, K., Bowie, D., and Traynelis, S. F. (1999). The glutamate receptor ion channel. *Pharmacol Rev* **51**, 1-61.
- Erreger, K., and Traynelis, S. F. (2005). Allosteric interaction between zinc and glutamate binding domains on NR2A causes desensitization of NMDA receptors. *J Physiol* **569**, 381-393.
- Fayyazuddin, A., Villaroel, A., Le Goff, A., Lerma, J., and Neyton, J. (2000). Four residues of the extracellular N-terminal domain of the NR2A subunit control high-affinity Zn²⁺ binding to NMDA receptors. *Neuron* **25**, 683-694.
- Fersht, A. R. (1999). *Structure and Mechanism in Protein Science: Guide to Enzyme Catalysis and Protein Folding*, Freeman edn (New York).
- Furukawa, H., Singh, S. K., Mancusso, R., and Gouaux, E. (2005). Subunit arrangement and function in NMDA receptors. *Nature* **438**, 185-192.
- Hatton, C. J., and Paoletti, P. (2005). Modulation of triheteromeric NMDA receptors by N-terminal domain ligands. *Neuron* **46**, 261-274.
- Horning, M. S., and Mayer, M. L. (2004). Regulation of AMPA receptor gating by ligand binding core dimers. *Neuron* **41**, 379-388.
- Ihle, E. C., and Patneau, D. K. (2000). Modulation of alpha-amino-3-hydroxy-5-methyl-4-isoxazolepropionic acid receptor desensitization by extracellular protons. *Mol Pharmacol* **58**, 1204-1212.
- Jin, R., Banke, T. G., Mayer, M. L., Traynelis, S. F., and Gouaux, E. (2003). Structural basis for partial agonist action at ionotropic glutamate receptors. *Nat Neurosci* **6**, 803-810.
- Jingami, H., Nakanishi, S., and Morikawa, K. (2003). Structure of the metabotropic glutamate receptor. *Curr Opin Neurobiol* **13**, 271-278.
- Kuusinen, A., Abele, R., Madden, D. R., and Keinanen, K. (1999). Oligomerization and ligand-binding properties of the ectodomain of the alpha-amino-3-hydroxy-5-methyl-4-isoxazole propionic acid receptor subunit GluRD. *J Biol Chem* **274**, 28937-28943.
- Kew, J. N., Trube, G., and Kemp, J. A. (1996). A novel mechanism of activity-dependent NMDA receptor antagonism describes the effect of ifenprodil in rat cultured cortical neurones. *J Physiol* **497** (Pt 3), 761-772.
- Lei, S., Orser, B. A., Thatcher, G. R., Reynolds, J. N., and MacDonald, J. F. (2001). Positive allosteric modulators of AMPA receptors reduce proton-induced receptor desensitization in rat hippocampal neurons. *J Neurophysiol* **85**, 2030-2038.

- Low, C. M., Lyuboslavsky, P., French, A., Le, P., Wyatte, K., Thiel, W. H., Marchan, E. M., Igarashi, K., Kashiwagi, K., Gernert, K., *et al.* (2003). Molecular determinants of proton-sensitive N-methyl-D-aspartate receptor gating. *Mol Pharmacol* 63, 1212-1222.
- Low, C. M., Zheng, F., Lyuboslavsky, P., and Traynelis, S. F. (2000). Molecular determinants of coordinated proton and zinc inhibition of N-methyl-D-aspartate receptors. *PNAS* 97, 11062-11067.
- Madry, C., Mesic, I., Betz, H., and Laube, B. (2007). The N-terminal domains of both NR1 and NR2 subunits determine allosteric Zn²⁺ inhibition and glycine affinity of NMDA receptors. *Mol Pharmacol*.
- Mayer, M. L. (2006). Glutamate receptors at atomic resolution. *Nature* 440, 456-462.
- Meddows, E., Le Bourdelles, B., Grimwood, S., Wafford, K., Sandhu, S., Whiting, P., and McIlhinney, R. A. (2001). Identification of molecular determinants that are important in the assembly of N-methyl-D-aspartate receptors. *J Biol Chem* 276, 18795-18803.
- O'Neil, K. T., and DeGrado, W. F. (1990). A thermodynamic scale for the helix-forming tendencies of the commonly occurring amino acids. *Science* 250, 646-651
- Paoletti, P., Ascher, P., and Neyton, J. (1997). High-affinity zinc inhibition of NMDA NR1-NR2A receptors. *J Neurosci* 17, 5711-5725.
- Paoletti, P., and Neyton, J. (2007). NMDA receptor subunits: function and pharmacology. *Curr Opin Pharmacol* 7, 39-47.
- Paoletti, P., Neyton, J., and Ascher, P. (1995). Glycine-independent and subunit-specific potentiation of NMDA responses by extracellular Mg²⁺. *Neuron* 15, 1109-1120.
- Paoletti, P., Perin-Dureau, F., Fayyazuddin, A., Le Goff, A., Callebaut, I., and Neyton, J. (2000). Molecular organization of a zinc binding N-terminal modulatory domain in a NMDA receptor subunit. *Neuron* 28, 911-925.
- Plested, A. J., and Mayer, M. L. (2007). Structure and mechanism of kainate receptor modulation by anions. *Neuron* 53, 829-841.
- Perin-Dureau, F., Rachline, J., Neyton, J., and Paoletti, P. (2002). Mapping the binding site of the neuroprotectant ifenprodil on NMDA receptors. *J Neurosci* 22, 5955-5965.
- Priel, A., Selak, S., Lerma, J., and Stern-Bach, Y. (2006). Block of kainate receptor desensitization uncovers a key trafficking checkpoint. *Neuron* 52, 1037-1046.
- Rachline, J., Perin-Dureau, F., Le Goff, A., Neyton, J., and Paoletti, P. (2005). The micromolar zinc-binding domain on the NMDA receptor subunit NR2B. *J Neurosci* 25, 308-317.
- Sine, S. M., and Engel, A. G. (2006). Recent advances in Cys-loop receptor structure and function. *Nature* 440, 448-455.
- Smart, T. G., Hosie, A. M., and Miller, P. S. (2004). Zn²⁺ ions: modulators of excitatory and inhibitory synaptic activity. *Neuroscientist* 10, 432-442.
- Sun, Y., Olson, R., Horning, M., Armstrong, N., Mayer, M., and Gouaux, E. (2002). Mechanism of glutamate receptor desensitization. *Nature* 417, 245-253.
- Traynelis, S. F., and Chesler, M. (2001). Proton release as a modulator of presynaptic function. *Neuron* 32, 960-962.
- Traynelis, S. F., and Cull-Candy, S. G. (1991). Pharmacological properties and H⁺ sensitivity of excitatory amino acid receptor channels in rat cerebellar granule neurones. *J Physiol* 433, 727-763.
- Vogt, K., Mellor, J., Tong, G., and Nicoll, R. (2000). The actions of synaptically released zinc at hippocampal mossy fiber synapses. *Neuron* 26, 187-196.

- Westbrook, G. L., and Mayer, M. L. (1987). Micromolar concentrations of Zn²⁺ antagonize NMDA and GABA responses of hippocampal neurons. *Nature* 328, 640-643.
- Weston, M. C., Schuck, P., Ghosal, A., Rosenmund, C., and Mayer, M. L. (2006). Conformational restriction blocks glutamate receptor desensitization. *Nat Struct Mol Biol* 13, 1120-1127.
- Zheng, F., Erreger, K., Low, C. M., Banke, T., Lee, C. J., Conn, P. J., and Traynelis, S. F. (2001). Allosteric interaction between the amino terminal domain and the ligand binding domain of NR2A. *Nat Neurosci* 4, 894-901.

FIGURE LEGENDS

Figure 1. The heterodimeric organization of ABDs in NR1/NR2A NMDA receptors.

A Left: Schematic representation of the domain organization of NMDA receptors. CTD: intracellular C-terminal domain; TMD: transmembrane domain that comprises the ion-channel pore; ABD: agonist binding domain that binds glycine (or D-serine) in NR1 and glutamate in NR2 subunits; NTD: N-terminal domain that forms in NR2A a modulatory domain binding with high affinity the allosteric inhibitor zinc. An intact receptor is believed to form a tetrameric complex assembled as a dimer of dimers. Right: Side and top views of the NR1/NR2A ABD heterodimer crystal structure (Furukawa et al., 2005). Helices α D and α J, which form the main interaction surfaces at the interface between the two partner subunits, are labeled. Note that interactions between the two subunits involve almost exclusively residues from lobes 1. **B** Amino acid sequence alignment of the ABD segments that form the dimer interface contacts in NMDA, AMPA and kainate receptors. On top, secondary structure assignment for NR1 and NR2A (α -helices in orange and β -sheet in blue) is shown. Amino acids directly contacting the agonist molecule (glutamate, or glycine for NR1 and NR3 subunits) are marked with an asterisk, while conserved residues are indicated by grey boxes. Boxed residues indicate positions that were mutated in the present study.

Figure 2. Disrupting the hydrophobic cores of the ABD dimer interface generates receptors with enhanced zinc sensitivity.

A Magnified views of the two hydrophobic clusters that form major sites of subunit-subunit contact in the NR1/NR2A ABD dimer interface. Homologous residues NR1-L777 (site A) and NR2A-L780 (site B), each on helix J, are at the center of a hydrophobic cluster, contacting through Van der Waals interactions the other residues at each site displayed in the yellow stick representation. Site A and site B are related by the pseudo two-fold molecular symmetry of the dimer assembly. **B** Comparison of current traces obtained from oocytes expressing either wild-type (wt) NR1/NR2A receptors, mutated NR1-L777A/NR2Awt receptors or NR1wt/NR2A-L780A receptors. Zinc was applied at increasing concentrations (5, 50 and 500 nM) during an application of 100 μ M glutamate and 100 μ M glycine. **C** Zinc inhibition concentration-response curves for NR1-L777A/NR2Awt ($\text{Inhib}_{\text{max}} = 99\%$, $\text{IC}_{50} = 1.1$ nM, $n_{\text{H}} = 0.94$, [n = 5]) and NR1wt/NR2A-L780A ($\text{Inhib}_{\text{max}} = 97\%$, $\text{IC}_{50} = 1.2$ nM, $n_{\text{H}} = 0.97$, [n = 5]) mutant receptors compared with wt receptor (dashed line; $\text{Inhib}_{\text{max}} = 81\%$, $\text{IC}_{50} = 6.9$ nM, $n_{\text{H}} = 1.02$, [n = 5]). Note that in wt receptors, zinc inhibition is partial while in the mutant receptors it is almost total.

Figure 3. Disruption of a dimer interface hydrogen bond network increases zinc sensitivity.

A Located at the base of helix J, site A residue NR1-E781 contributes to the ABD dimer formation by making two contacts with the adjacent NR2A subunit: a hydrogen bond with the N α of NR2A-E516, and an “indirect” hydrogen bond with the N α of NR2A-E517 via a water molecule (shown as a red ball). **B** Zinc inhibition concentration-response curve for NR1-E781Q/NR2Awt mutant receptors (Inhib_{max} = 97%, IC₅₀ = 1.4 nM, n_H = 1.01, [n = 3]) compared with wild-type receptors (dashed line; Inhib_{max} = 81%, IC₅₀ = 6.9 nM, n_H = 1.02, [n = 5]).

Figure 4. Redox-controlled switch from low to high zinc sensitivity in receptors containing disulfide bond cross-linked ABDs.

A Top view of the NR1/NR2A ABD dimer highlighting the four cysteines introduced at the dimer interface to form intersubunit disulphide bonds (sulfurs are shown in yellow; Furukawa et al., 2005). **B** Inhibition by increasing zinc concentrations (5, 50 and 500 nM) of currents carried by NR1-CC/NR2A-CC receptors expressed in a single oocyte under control conditions and treated sequentially with DTNB (0.5 mM, 5 min), DTE (5 mM, 15 min), DTNB (second round, same concentration, 45 min) and DTE (second round, same concentration, 15 min). **C**, Zinc inhibition concentration-response curves for NR1-CC/NR2A-CC receptors in control condition (Inhib_{max} = 64%, IC₅₀ = 6.0 nM, n_H = 0.58), after DTNB treatment (Inhib_{max} = 37%, IC₅₀ = 3.7 nM, n_H = 0.37) and after a subsequent DTE treatment (Inhib_{max} = 100%, IC₅₀ = 2.0 nM, n_H = 0.63). Each point is the mean value from 5 to 12 cells. **D**, Bar graph showing the residual current at 500 nM zinc (I_{res}) in control conditions, after DTNB treatment and after a subsequent DTE treatment, for wt NR1/NR2A receptors (I_{res} = 21 ± 0.7 % [n = 4]; 25 ± 0.9 % [n = 4]; 26 ± 1.4 % [n = 4]), NR1-CC/NR2Awt receptors (I_{res} = 9 ± 1 % [n = 6]; 8 ± 1 % [n = 6]; 12 ± 1 % [n = 5]), NR1wt/NR2A-CC receptors (I_{res} = 7 ± 0.4 % [n = 4]; 11 ± 2 % [n = 4]; 6 ± 0.8 % [n = 4]), and NR1-CC/NR2A-CC receptors (I_{res} = 40 ± 2.4 % [n = 12]; 67 ± 3.6 % [n = 11]; 3.6 ± 0.9 % [n = 9]). For these latter receptors, a second round of consecutive DTE and DTNB treatments was performed (I_{res} = 61 ± 0.8 % [n = 4]; 2.7 ± 0.6 % [n = 4], respectively) revealing the reversibility of the redox-induced effects on zinc sensitivity.

Figure 5. Disrupting the hydrophobic cores of the ABD dimer interface generates receptors with greatly enhanced proton sensitivity.

A Recordings showing the potentiating effects induced by alkalinization of the external solution on currents carried by wt NR1/NR2A receptors or mutated NR1-L777A/NR2Awt, NR1wt/NR2A-L780A and NR1wt/NR2A-L780F receptors. During an application of glutamate and glycine (100 μ M each), pH was switched transiently from pH 7.3 to the indicated value. **B** Proton inhibition concentration-response curves of NR1-L777A/NR2Awt ($pH_{IC50} = 9.13$, $n_H = 0.83$, [n = 4-7]), NR1wt/NR2A-L780A ($pH_{IC50} = 9.16$, $n_H = 0.81$, [n = 4-8]) and NR1wt/NR2A-L780F receptors ($pH_{IC50} = 9.08$, $n_H = 0.97$, [n = 4]). For comparison, the proton sensitivity of wt NR1/NR2A receptors is also shown (dashed line; $pH_{IC50} = 6.92$, $n_H = 1.69$, [n = 4]).

Figure 6. Strong correlation between pH and zinc sensitivities at NR1/NR2A receptors.

The change in free-energy between the zinc-bound active and inactive states ($\Delta\Delta G^\circ_{Zn}$; an index of the maximal level of zinc inhibition; see Experimental Procedures) is plotted versus the change in free-energy between the proton bound and unbound states ($\Delta\Delta G^\circ_{pH}$; an index of the pH sensitivity; see Experimental Procedures) for wt and 22 interface mutant receptors. Coordinates of wt NR1/NR2A receptors are (0,0) (open circle). The line represents a linear regression fit of the data points. The R value of the fit is 0.85. Numbers refer to the following mutant receptors: 1 = NR1wt/NR2A-I514A; 2 = NR1-I519F/NR2Awt; 3 = NR1-I519A/NR2Awt; 4 = NR1-L774A/NR2Awt; 5 = NR1-A524D/NR2Awt; 6 = NR1wt/NR2A-V526A; 7 = NR1-I519A/NR2A-I514A; 8 = NR1-E781D/NR2Awt; 9 = NR1wt/NR2A-L777A; 10 = NR1-E781A/NR2Awt; 11 = NR1-A524E/NR2Awt; 12 = NR1wt/NR2A-V526K; 13 = NR1-A524K/NR2Awt; 14 = NR1-L774A/NR2A-L777A; 15 = NR1-L777C/NR2Awt; 16 = NR1wt/NR2A-L780C; 17 = NR1-E781Q/NR2Awt; 18 = NR1wt /NR2A-L780S; 19 = NR1-L777F/NR2Awt; 20 = NR1wt/NR2A-L780A; 21 = NR1-L777A/NR2Awt; 22 = NR1-L777S/NR2Awt. Data from NR1-I519D/NR2Awt receptors were excluded from this plot because H^+ IC_{50} could not be accurately measured for these receptors (see Results).

Figure 7. MTSES Modification rate of NR1wt/NR2A-V526C receptors is increased by zinc.

A Recording showing the inhibitory effect of 2 mM MTSES on currents carried by NR1wt/NR2A-V526C receptors. NMDAR currents were induced by 100 μ M glutamate and 100 μ M glycine in the absence of zinc (no added zinc plus 10 μ M DTPA). **B** Same protocol as in **A** (but different cell) except that 500 nM free zinc was present throughout the experiment. **C** Comparison of the inhibition kinetics of MTSES in the presence and absence of extracellular zinc. Current traces from cells shown in **A** and **B** were normalized and fitted with a bi-exponential function (dashed lines). The values of τ_{fast} and τ_{slow} and their relative

weight were 1.4 sec (41%) and 35.4 sec (59%) in the absence of zinc (plus DTPA) and 1.3 sec (44%) and 11.9 sec (56%) in zinc, respectively. Note that the fast component is likely to reflect MTSES modification of an endogenous cysteine and not of 2A-V526C since a similar fast component of inhibition is also seen on wild-type NR1/NR2A receptors (while the slow component is not). **D** Mean time constants of the slow component of MTSES inhibition recorded in the absence of zinc (no added zinc plus DTPA) or in its presence and measured as shown in C. The values of τ_{slow} are 28.5 ± 4.9 sec ($-\text{Zn}^{2+}$, $n = 5$) and 15.0 ± 2.1 sec ($+\text{Zn}^{2+}$, $n = 4$) (***: $p < 0.005$, Student's t-test).

Figure 8. Proposed model for allosteric modulation of NR1/NR2A receptors.

Shown are two subunits forming a functional dimeric unit. An intact NMDA receptor is believed to assemble as a dimer of dimers. For additional details concerning the model, see Discussion.

SUPPLEMENTARY DATA

Figure S1. Mutations aimed at stabilizing the ABD dimer interface through hydrogen bonds decrease zinc and pH sensitivities.

Comparison of the zinc (Left) and proton (Right) sensitivities of NR1-E522Q/NR2A-G784E (circles, solid line) with wt NR1/NR2A receptors (open squares, dashed line). For zinc inhibition, $\text{Inhib}_{\text{max}}$, IC_{50} and n_{H} values are: 71%, 15.7 nM and 0.85 [$n = 4$] for mutant receptors, and 81%, 10.5 nM and 0.91 [$n = 5$] for wt receptors. For proton inhibition, $\text{pH}_{\text{IC}_{50}}$ and n_{H} values are 6.82 and 1.95 [$n = 5$] for mutant receptors and 6.92 and 1.69 [$n = 14$] for wt receptors.

Figure S2. Intersubunit disulfide bond formation in receptors with cysteine mutations at the ABD NR1/NR2A dimer interface.

Western blots using an anti-NR1 antibody on membrane fractions of *Xenopus* oocytes expressing three different combinations of wt or cysteine mutated NR1 and NR2A subunits (NR1-CC and NR2A-CC, see Fig. 4). Samples were run in the presence (reduced) or absence (non-reduced) of DTE. The expected molecular weight of NR1 monomers is ~110 kDa while that of NR1/NR2A dimers is expected to be ~300 kDa. Note that an intense band of high molecular weight, likely corresponding to disulfide-linked NR1/NR2A heterodimers, is only seen in non-reducing conditions when both subunits are mutated.

Figure S3. Synergistic effect on proton sensitivity of an NR2A-NTD deletion combined with an ABD dimer interface mutation.

Proton inhibition concentration-response curves of NR1-E781A/NR2A-deINTD (filled circles, black line; $\text{pH}_{\text{IC}_{50}} = 9.05$, $n_{\text{H}} = 0.85$, [$n = 4$]), NR1-E781A/NR2Awt receptors (open circles, dashed black line; $\text{pH}_{\text{IC}_{50}} = 7.26$, $n_{\text{H}} = 1.13$, [$n = 4$]), NR1wt/NR2A-deINTD (filled squares, gray line; $\text{pH}_{\text{IC}_{50}} = 7.16$, $n_{\text{H}} = 1.16$, [$n = 5$]) and wt NR1/NR2A receptors (open squares, dashed gray line; $\text{pH}_{\text{IC}_{50}} = 6.92$, $n_{\text{H}} = 1.69$, [$n = 4$]). Note that while the ABD dimer interface point mutation or the NR2A-NTD deletion have little effect on pH sensitivity on their own, the combination of both modifications strongly increases pH sensitivity.

Figure S4. Mutations NR1-L777A and NR2A-L780A have only minor effects on glutamate and glycine sensitivities.

A Agonist concentration-response curves of NR1-L777A/NR2Awt (circles, solid line) and wt NR1/NR2A receptors (open squares, dashed line). Left: glutamate concentration-response curves in the presence of 100 μ M glycine. EC_{50} and Hill coefficient values are: $2.9 \pm 0.3 \mu$ M and 1.1 [n = 4] for mutant receptors, and $4.6 \pm 0.2 \mu$ M and 1.3 [n = 2] for wt receptors. Right: glycine concentration-response curves in the presence of 100 μ M glutamate. The values of EC_{50} and Hill coefficient are: $2.3 \pm 0.2 \mu$ M and 1.1 [n = 5] for mutant receptors, and $1.2 \pm 0.1 \mu$ M and 1.4 [n = 7] for wt receptors. **B** Agonist concentration-response curves of NR1wt/NR2A-L780A (circles, solid line) and wt NR1/NR2A receptors (open squares, dashed line). Left: glutamate concentration-response curves in the presence of 100 μ M glycine. For mutant receptors, EC_{50} and Hill coefficient values are $2.0 \pm 0.2 \mu$ M and 1.1 [n = 4]. Right: glycine concentration-response curves in the presence of 100 μ M glutamate. For mutant receptors, EC_{50} and Hill coefficient are $3.4 \pm 0.2 \mu$ M and 1.1 [n = 4]. EC_{50} and n_H values for wt receptors are the same as in A (wt data replotted from A).

Figure S5. Mutating residue NR2A-I514 strongly decreases glutamate affinity.

A Agonist concentration-response curves of NR1wt/NR2A-I514A (circles, solid line) and wt NR1/NR2A (open squares, dashed line) receptors. Left: glutamate concentration-response curves in the presence of 100 μ M glycine. EC_{50} and Hill coefficient values are: $77.8 \pm 1.6 \mu$ M and 1.5 [n = 5] for mutant receptors, and $4.6 \pm 0.2 \mu$ M, 1.3 [n = 2] for wt receptors. Right: glycine concentration-response curves in the presence of 100 μ M glutamate. The values of EC_{50} and Hill coefficient are: $1.3 \pm 0.2 \mu$ M, 1.1 [n = 3] for mutant receptors, and $1.2 \pm 0.1 \mu$ M and 1.4 [n = 7] for wt receptors. **B** Agonist concentration-response curves of NR1wt/NR2A-I514D (circles, solid line) and wt NR1/NR2A (open squares, dashed line) receptors. Left: glutamate concentration-response curves in the presence of 100 μ M glycine. For mutant receptors, EC_{50} and Hill coefficient values are $319 \pm 7 \mu$ M and 1.5 [n = 3]. Right: glycine concentration-response curves in the presence of 100 μ M glutamate. For mutant receptors, EC_{50} and Hill coefficient are $1.2 \pm 0.3 \mu$ M and 0.8 [n = 3]. EC_{50} and n_H values for wt receptors are the same as in A (wt data replotted from A).

Figure S6. Effects of the redox treatments on glutamate and glycine sensitivities of NR1-CC/NR2A-CC mutant receptors.

Agonist concentration-response curves of NR1-CC/NR2A-CC (circles, solid line) in control conditions, after DTNB treatment (0.5 mM, 5 min) and after subsequent DTE treatment (5 mM, 15 min). Glutamate concentration-response curves (left panels) were performed in 1 mM glycine while glycine concentration-response curves (right panels) were performed in 1

mM glutamate. **A** Control conditions e. before any redox treatment). Data obtained on wt NR1/NR2A receptors are also shown (open squares, dashed line). For glutamate, EC_{50} and Hill coefficient values are: $32.5 \pm 2.0 \mu\text{M}$ and 1.1 [n = 3] for mutant receptors, and $4.6 \pm 0.2 \mu\text{M}$ and 1.3 [n = 2] for wt receptors. For glycine, EC_{50} and Hill coefficient values are: $22.6 \pm 1.0 \mu\text{M}$ and 1.1 [n = 3] for mutant receptors, and $1.2 \pm 0.1 \mu\text{M}$ and 1.4 [n = 7] for wt receptors. **B** After DTNB treatment. For glutamate, EC_{50} and Hill coefficient values are $24.6 \pm 2.1 \mu\text{M}$ and 1.1 [n = 3]. For glycine, EC_{50} and Hill coefficient values are $26.1 \pm 0.7 \mu\text{M}$ and 1.2 [n = 3]. **C** After DTE treatment. For glutamate, EC_{50} and Hill coefficient values are $7.7 \pm 0.1 \mu\text{M}$ and 0.9 [n = 3]. For glycine, EC_{50} and Hill coefficient values are $6.6 \pm 0.2 \mu\text{M}$ and 1.0 [n = 3].

Table 1. Effects of ABD dimer interface mutations on Zn²⁺ and H⁺ inhibitions of NR1/NR2A receptors

Mutant	Zn ²⁺ inhibition				H ⁺ inhibition		
	IC ₅₀ (nM)	Max. Inhib. (%)	n _H	# cells	pH IC ₅₀	n _H	#cells
wild-type	10.5 ± 0.8	81 ± 1	0.91	(5)	6.95 ± 0.05	1.69	(14)
NR1 mutant							
I519A	8.9 ± 2.1	84 ± 1 **	0.90	(4)	6.95 ± 0.01	1.72	(4)
I519D	2.5 ± 0.4 **	97 ± 1 **	0.98	(4)	a		
I519F	8.1 ± 0.1	82 ± 2	0.94	(3)	6.96 ± 0.02	1.60	(3)
I519V	11.7 ± 0.3	77 ± 1	0.84	(3)	6.95 ± 0.02	1.76	(4)
A524D	3.5 ± 0.2 **	90 ± 1 **	0.95	(7)	6.86 ± 0.02 **	1.68	(7)
A524E	2.8 ± 0.1 **	95 ± 1 **	1.00	(7)	7.01 ± 0.02 **	1.36	(5)
A524K	1.5 ± 0.1 **	94 ± 1 **	0.81	(4)	7.82 ± 0.04 **	1.01	(4)
K531A	16.4 ± 0.5 **	81 ± 1	0.95	(4)	7.00 ± 0.01 **	1.51	(4)
L774A	7.9 ± 0.7 *	84 ± 1 *	0.90	(7)	6.96 ± 0.02	1.52	(3)
L777A	1.1 ± 0.1 **	99 ± 1 **	0.94	(7)	9.13 ± 0.05 **	0.83	(4-7)
L777C	1.7 ± 0.1 **	97 ± 1 **	0.84	(7)	7.77 ± 0.05 **	0.91	(3)
L777F	0.9 ± 0.1 **	96 ± 1 **	0.85	(3)	9.18 ± 0.12 **	0.54	(4)
L777S	0.9 ± 0.1 **	98 ± 2 **	0.82	(3)	9.57 ± 0.07 **	0.60	(3)
K778A	15.9 ± 0.5 *	79 ± 1 *	0.89	(4)	6.90 ± 0.01	1.69	(4)
E781A	2.4 ± 0.1 **	92 ± 1 **	1.10	(9)	7.20 ± 0.06 **	1.22	(8)
E781D	7.4 ± 0.3 **	87 ± 1 **	0.90	(7)	7.14 ± 0.03 **	1.62	(4)
E781Q	1.3 ± 0.1 **	97 ± 1 **	1.00	(8)	8.18 ± 0.05 **	0.85	(4)
NR2A mutant							
I514A	8.9 ± 0.4	81 ± 1	0.83	(4)	6.97 ± 0.02	1.60	(4)
I514D	16.9 ± 0.2 **	87 ± 1 **	0.93	(4)	N.D. [#]		
V526A	8.4 ± 0.2 **	86 ± 1 **	0.98	(4)	7.02 ± 0.03 **	1.64	(9)
V526K	2.0 ± 0.2 **	94 ± 1 **	0.83	(10)	7.63 ± 0.04 **	1.47	(8)
L777A	2.0 ± 0.1 **	91 ± 1 **	0.90	(2)	7.19 ± 0.04 *	1.26	(3)
L780A	1.2 ± 0.1 **	97 ± 2 **	0.97	(6)	9.16 ± 0.10 **	0.81	(4-8)
L780C	1.2 ± 0.2 **	95 ± 1 **	0.85	(6)	8.16 ± 0.05 *	0.77	(2)
L780S	1.1 ± 0.2 **	96 ± 1 **	0.77	(3)	8.88 ± 0.01 **	0.59	(3)
L780F		N.D.			9.08 ± 0.03 **	0.97	(4)
Q781A	12.0 ± 0.9	81 ± 1	0.90	(4)	6.94 ± 0.02	1.67	(3)
NR1 mut. / NR2A mut.							
I519A / I514A	8.4 ± 0.5	88 ± 1 **	0.91	(4)	7.07 ± 0.03 **	1.46	(4)
N521Y / E516Y	10.5 ± 0.4	82 ± 1	1.00	(4)	N.D.		
E522Q / G784E	15.7 ± 0.8 *	71 ± 1 **	0.85	(4)	6.82 ± 0.01 **	1.95	(5)
A524E / V526K-D776N	1.6 ± 0.1 **	97 ± 2 **	0.91	(4)	N.D.		
S773N / S519E	11.3 ± 1.3	77 ± 2	0.99	(3)	6.95 ± 0.02	1.58	(2)
L774A / L777A	1.5 ± 0.1 **	93 ± 1 **	0.98	(4)	8.04 ± 0.06 **	0.72	(3)

a: NR1-I519D/NR2Awt receptors displayed a bell-shaped pH dose-response curve (see Results) ; N.D.: not determined; N.D.[#]: not determined because of a strong decrease in glutamate affinity (see Methods and Fig. S5) ; **p* < 0.05 ; ***p* < 0.01 compared with wild-type with Student's *t* test modified for unequal variances.

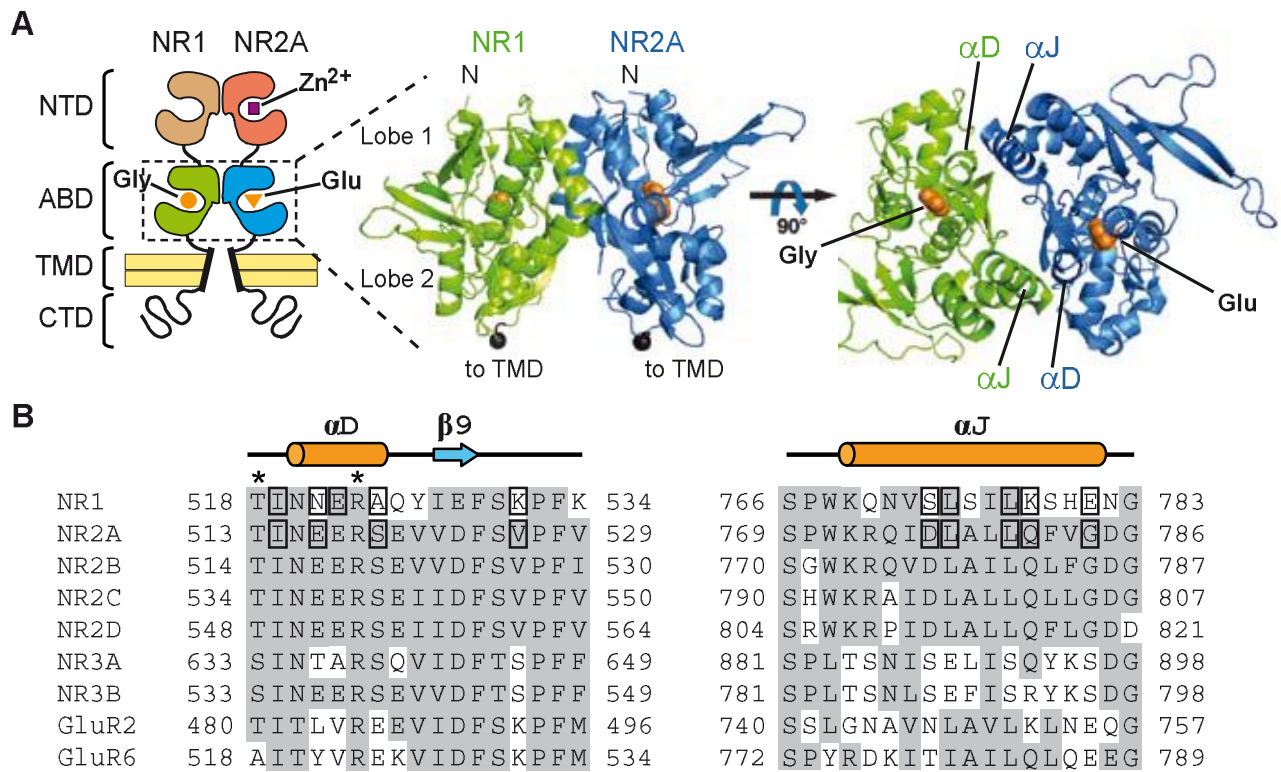


Figure 1

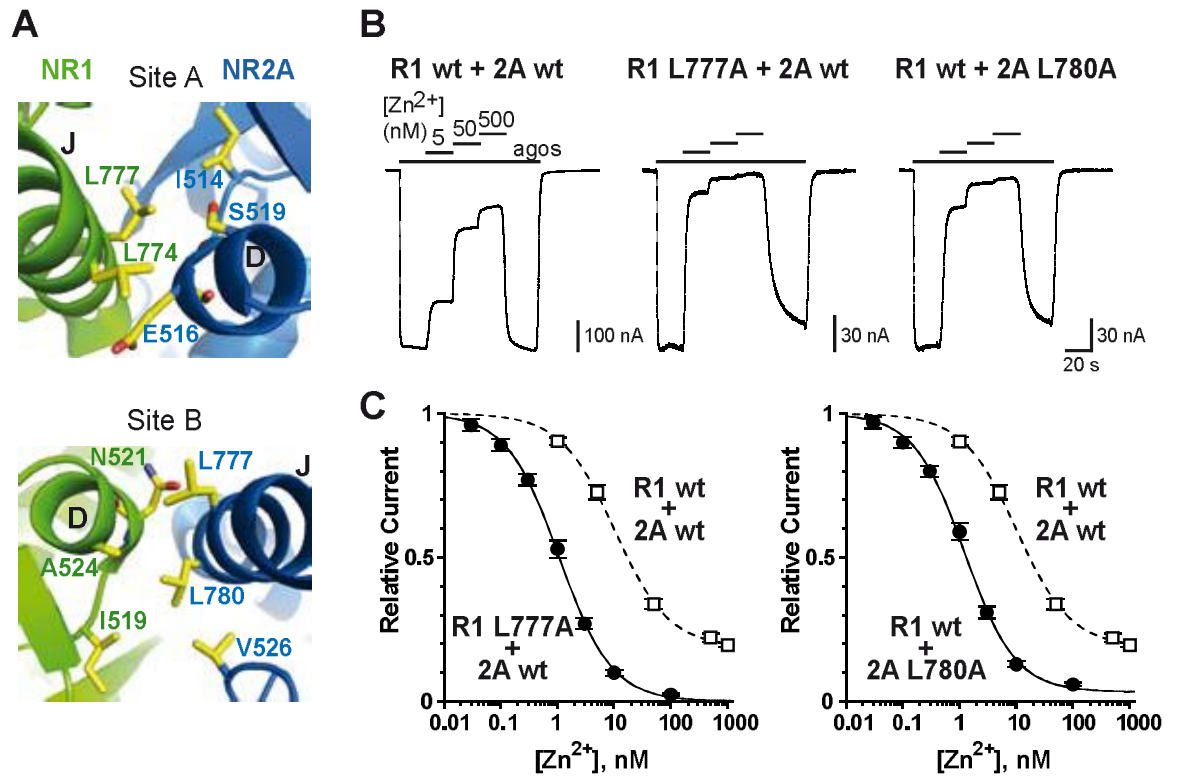


Figure 2

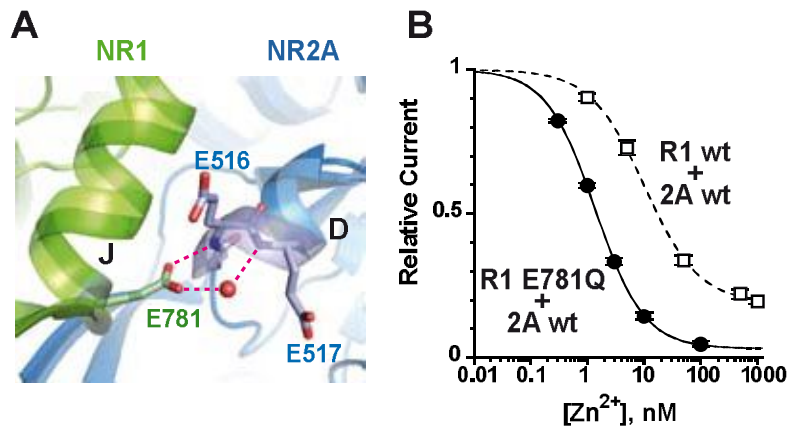


Figure 3

Figure

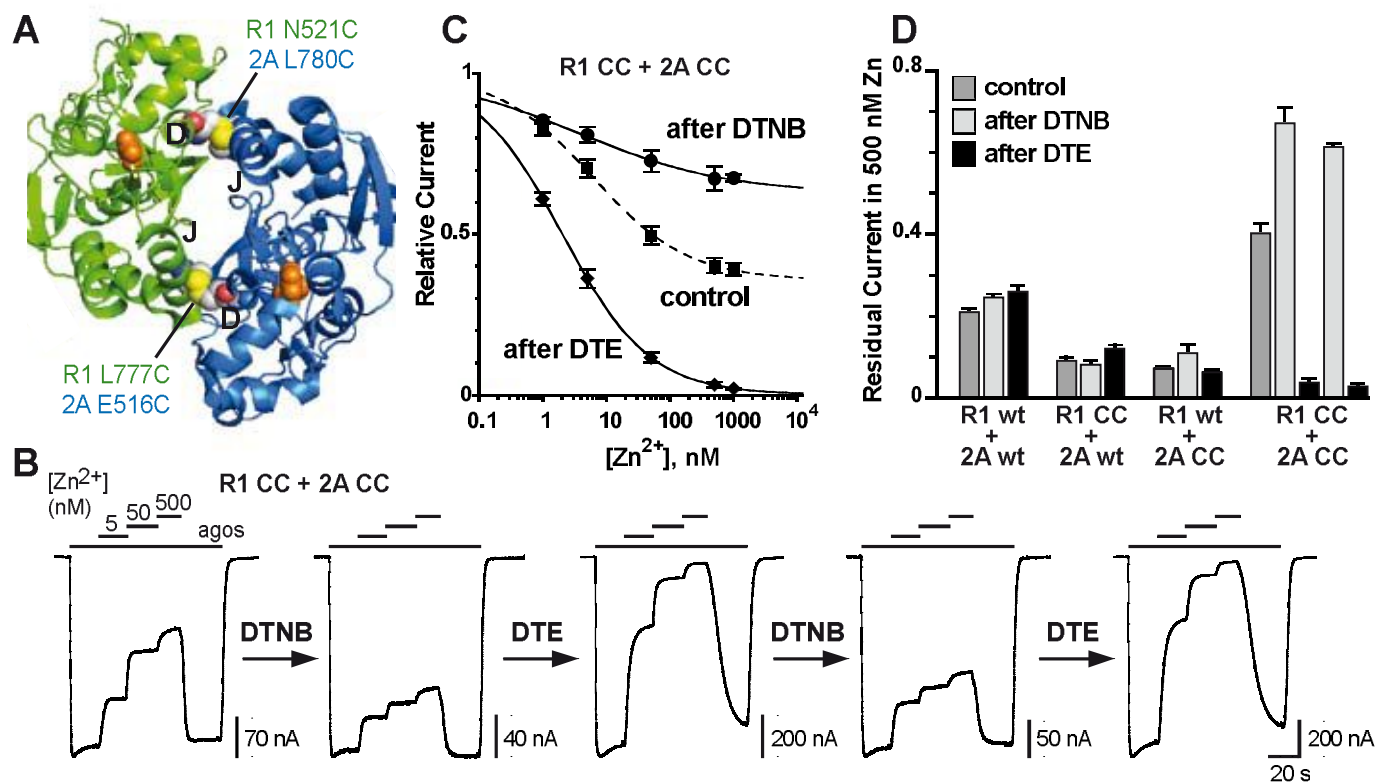


Figure 4

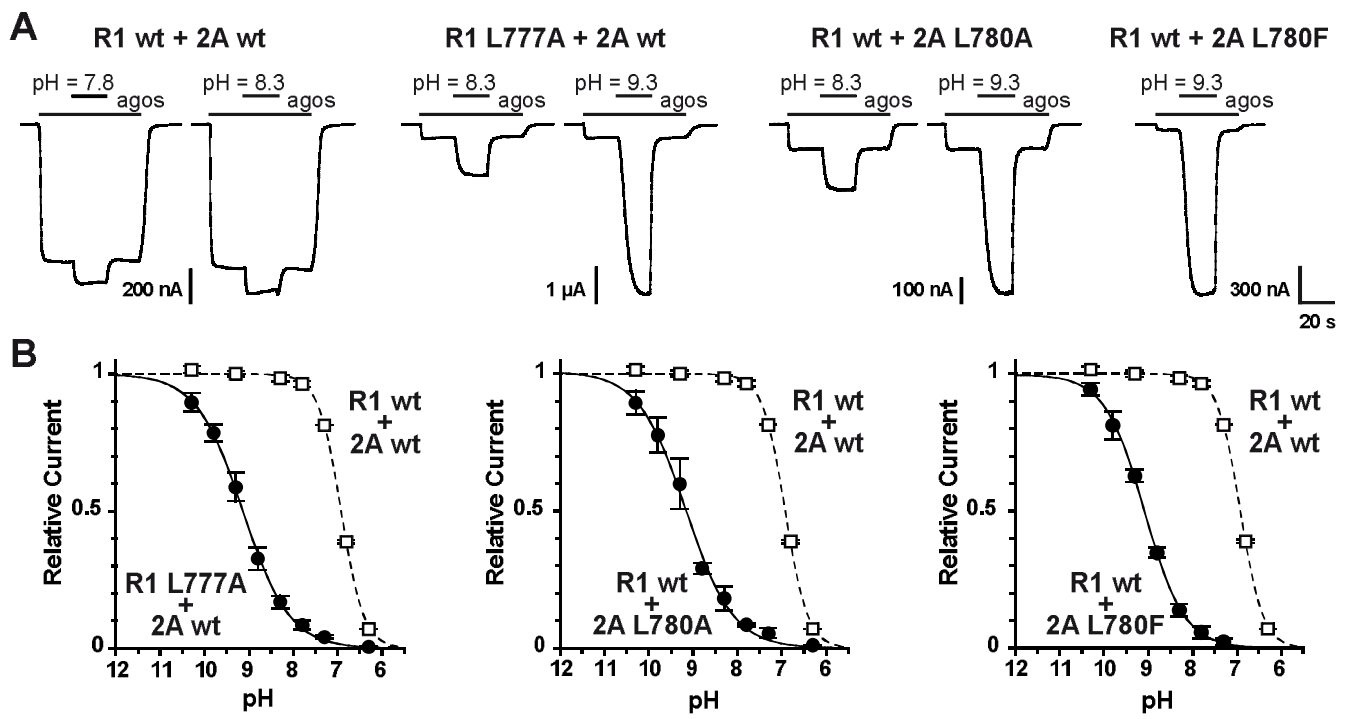


Figure 5

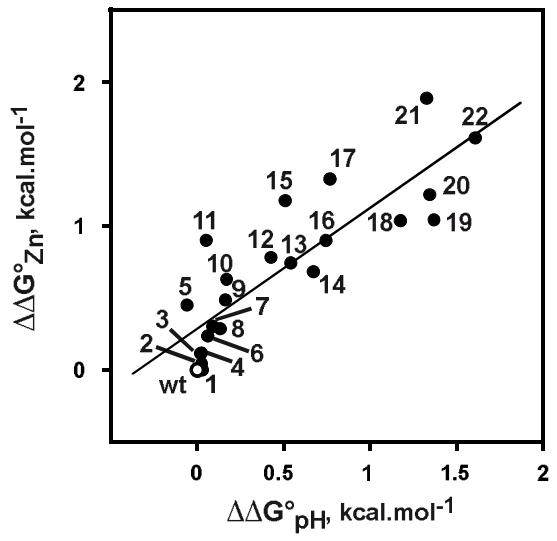


Figure 6

Figure

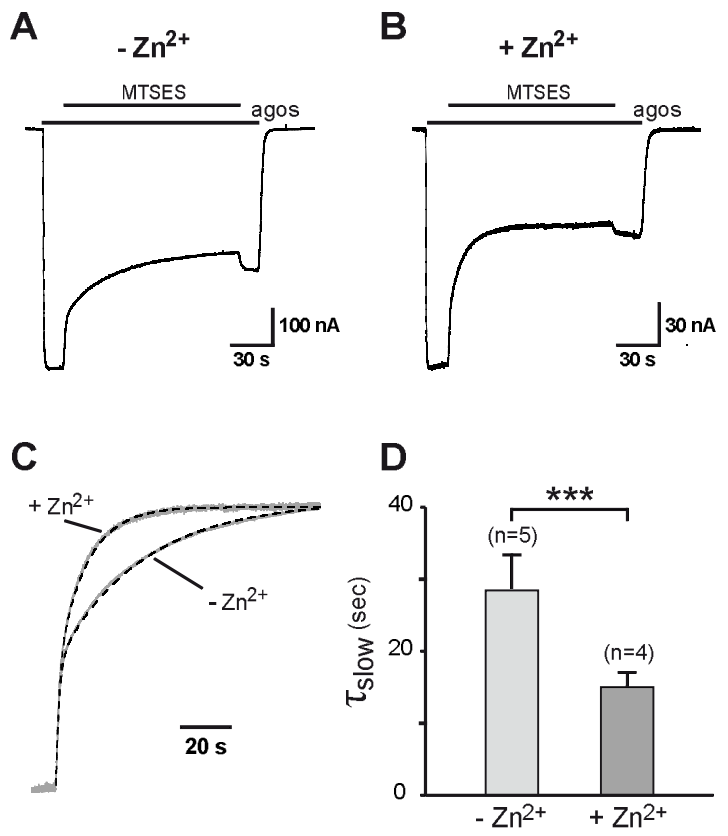


Figure 7

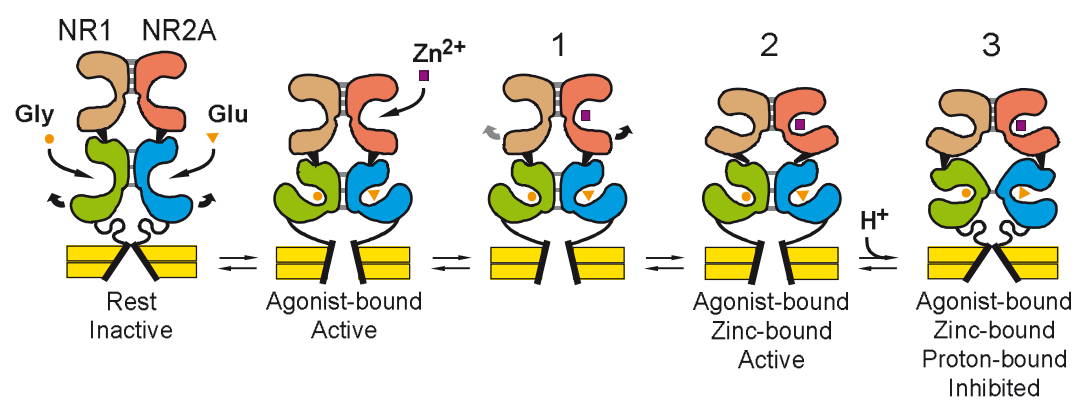


Figure 8

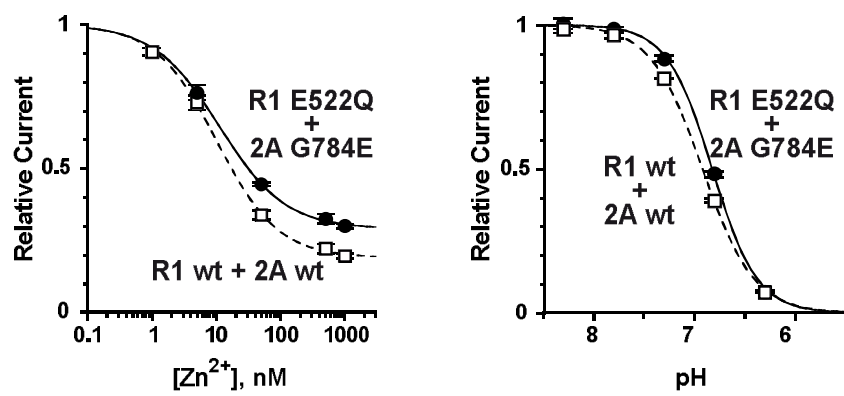


Figure S1

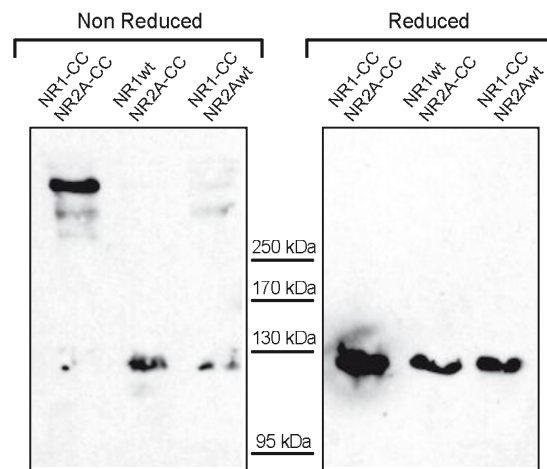


Figure S2

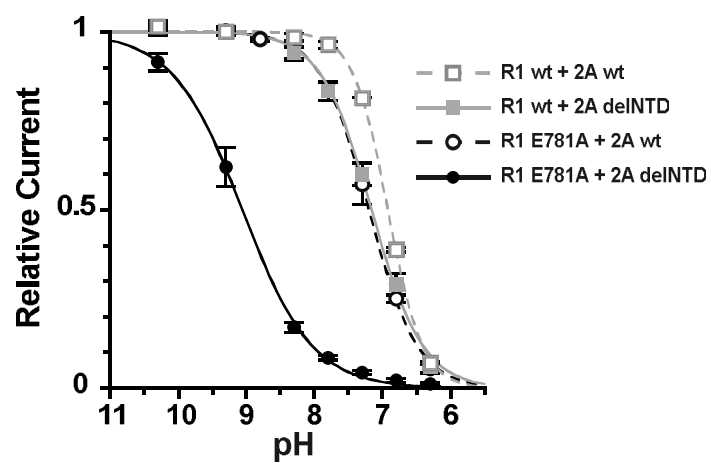


Figure S3

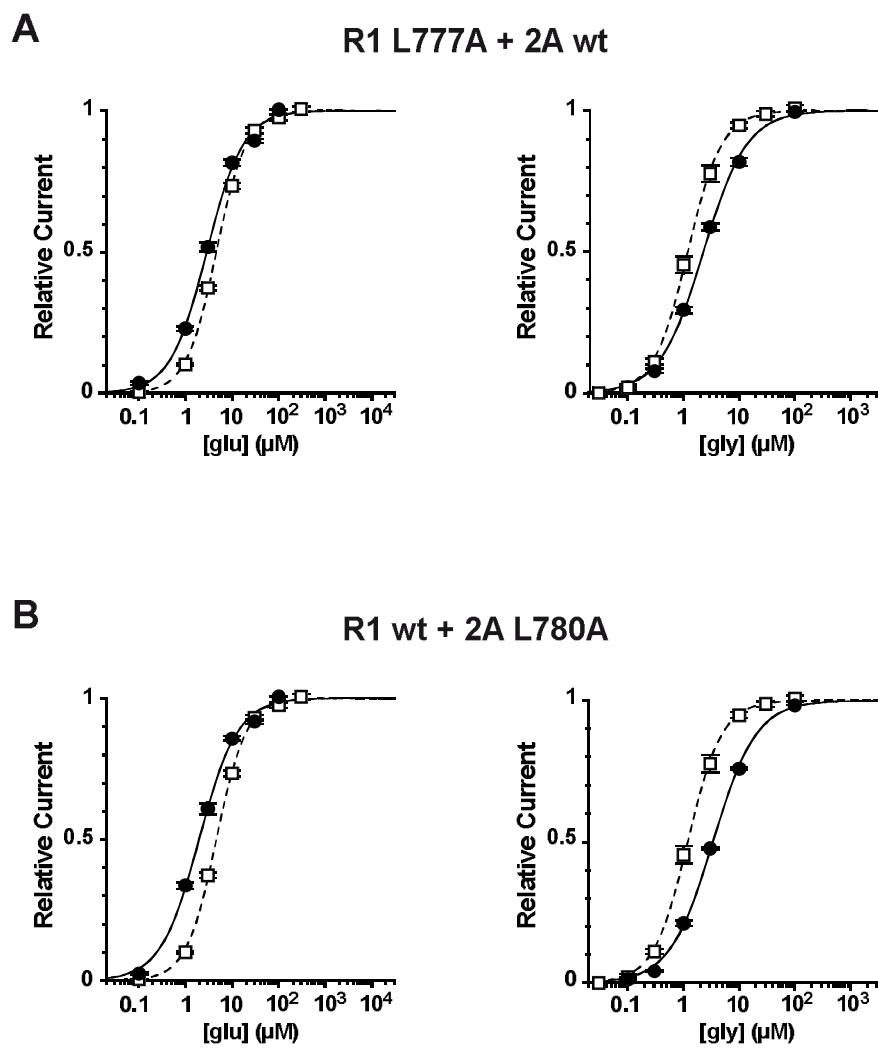


Figure S4

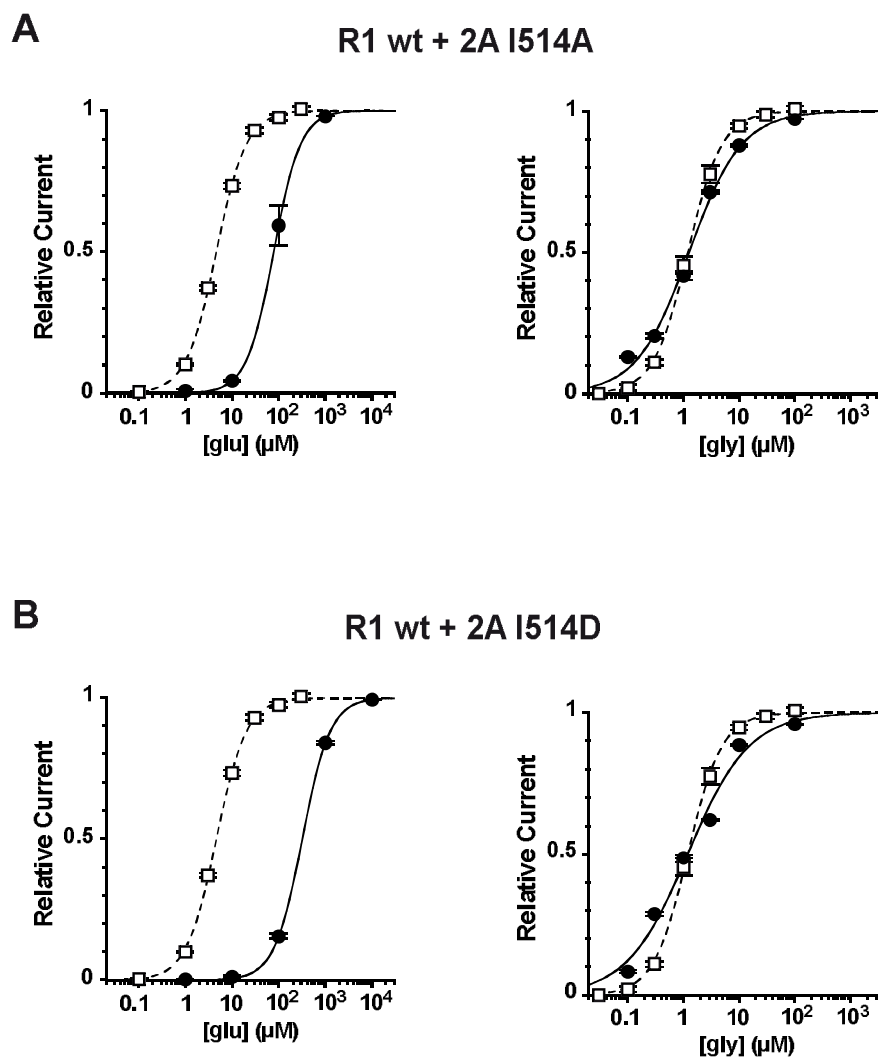


Figure S5

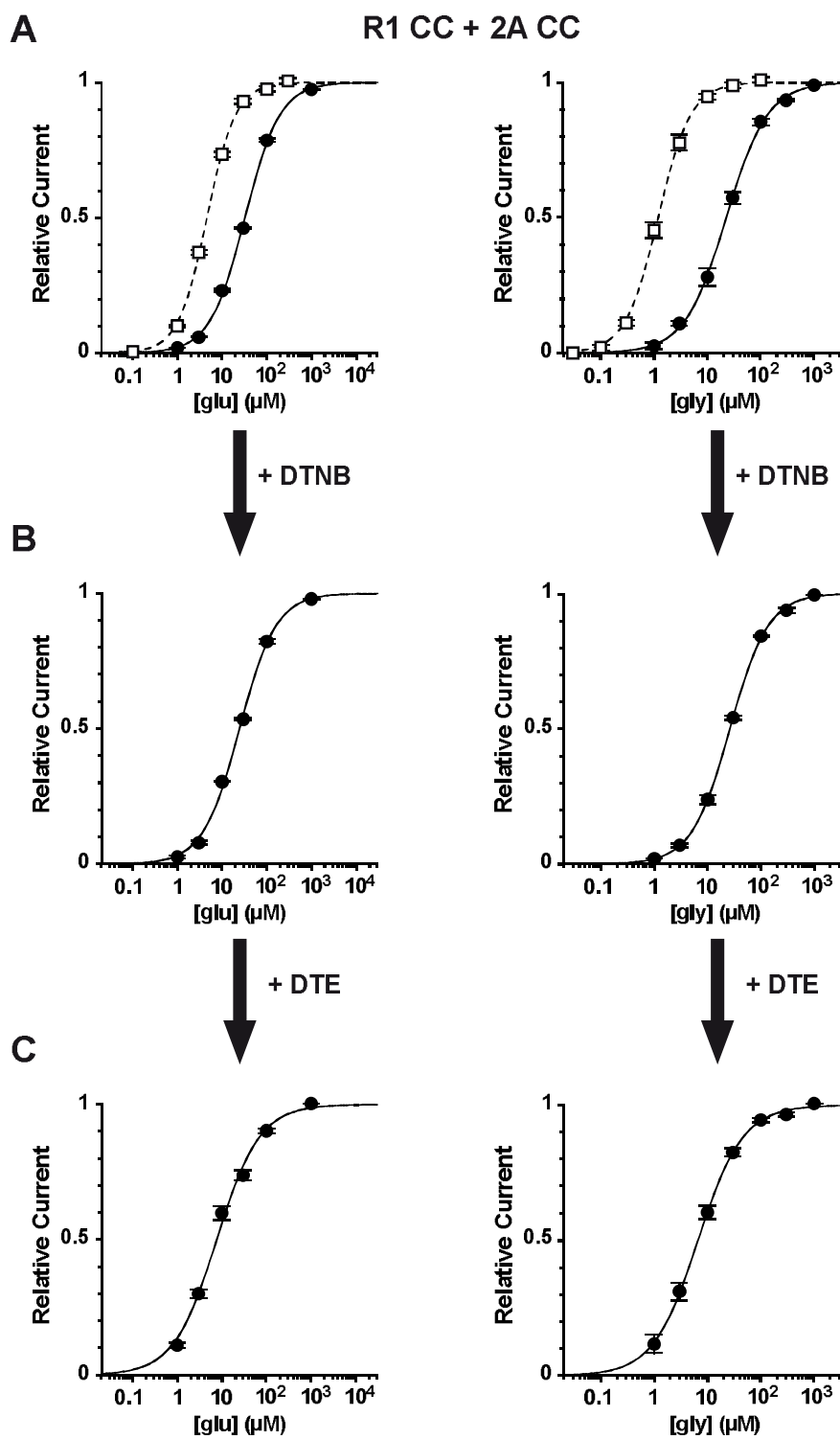


Figure S6